The Journal of Immunology

A *Brucella* spp. Protease Inhibitor Limits Antigen Lysosomal Proteolysis, Increases Cross-Presentation, and Enhances CD8$^+$ T Cell Responses

Lorena M. Coria, Andrés E. Ibañez, Mercedes Tkach, Florencia Sabbione, Laura Bruno, Marianela V. Carabajal, Paula M. Berguer, Paula Barrionuevo, Roxana Schillaci, Analía S. Trevani, Guillermo H. Giambartolomei, Karina A. Pasquevich and Juliana Cassataro

J Immunol published online 15 April 2016
http://www.jimmunol.org/content/early/2016/04/14/jimmunol.1501188

The Journal of Immunology is published twice each month by The American Association of Immunologists, Inc., 9650 Rockville Pike, Bethesda, MD 20814-3994.

Print ISSN: 0022-1767 Online ISSN: 1550-6606.

Published April 15, 2016, doi:10.4049/jimmunol.1501188

A *Brucella* spp. Protease Inhibitor Limits Antigen Lysosomal Proteolysis, Increases Cross-Presentation, and Enhances CD8$^+$ T Cell Responses

Lorena M. Coria,* Andrés E. Ibañez,* Mercedes Tkach,† Florencia Sabbione,‡ Laura Bruno,* Marianela V. Carabajal,* Paula M. Berguer,§ Paula Barrionuevo,‡ Roxana Schillaci,† Analía S. Trevani,‡ Guillermo H. Giambartolomei,¶ Karina A. Pasquevich,* and Juliana Cassataro*

In this study, we demonstrate that the unlipidated (U) outer membrane protein (Omp) 19 from *Brucella* spp. is a competitive inhibitor of human cathepsin L. U-Omp19 inhibits lysosome cathepsins and APC-derived microsome activity in vitro and partially inhibits lysosomal cathepsin L activity within live APCs. Codelivery of U-Omp19 with the Ag can reduce intracellular Ag digestion and increases Ag half-life in dendritic cells (DCs). U-Omp19 retains the Ag in Lamp-2$^+$ compartments after its internalization and promotes a sustained expression of MHC class I/peptide complexes in the cell surface of DCs. Consequently, U-Omp19 enhances Ag cross-presentation by DCs to CD8$^+$ T cells. U-Omp19 s.c. delivery induces the recruitment of CD11c$^+$CD8α$^+$ DCs and monocytes to lymph nodes whereas it partially limits in vivo Ag proteolysis inside DCs. Accordingly, this protein is able to induce CD8$^+$ T cell responses in vivo against codelivered Ag. Antitumor responses were elicited after U-Omp19 coadministration, increasing survival of mice in a murine melanoma challenge model. Collectively, these results indicate that a cysteine protease inhibitor from bacterial origin could be a suitable component of vaccine formulations against tumors. ***The Journal of Immunology*****, 2016, 196: 000–000.**

Adjuvants are compounds or molecules that increase the immune response to coadministered Ags in a vaccine formulation. Most adjuvants target dendritic cells (DCs), as they can activate naive T cells, initiating the course of the adaptive immune response (1). The duration and degree of Ag presentation determine the outcome of the T cell response (2–4). Moreover, Ag availability determines T cell–DC interaction kinetics and memory fate decisions (5).

Lysosomal proteases are crucial in many cellular processes such as Ag presentation by APCs (6–9). Besides, it has been reported that the extraordinary function of DCs as professional APCs could be explained by their particular moderate proteolytic activity (10). Consequently, protease-resistant Ags often elicit more robust immune responses (11, 12).

Ags can be processed in specialized endosomal compartments with mild proteolytic activity that favors cross-presentation (13–16). These observations support the idea that preserving or diverting Ags from lysosomal degradation increases Ag amount and availability to enter into the cytosolic pathway of cross-presentation. Cross-presentation involves the uptake and processing of exogenous Ags within the MHC class I (MHC I)–restricted pathway by APCs. The most important mechanism that explains this phenomenon relies on the capacity of Ags to escape from the endosomal compartments to the cytosol where they are degraded by the proteasome and transferred to the peptide-loading machinery of MHC I in the endoplasmic reticulum (17). This pathway is referred to as the cytosolic pathway and predominates in vivo. The degradative potential of lysosomes influences the amount of Ag that can reach the cytoplasm (10, 18).

*Instituto de Investigaciones Biotecnológicas–Instituto Tecnológico de Chascomús, Universidad Nacional de San Martín, Consejo Nacional de Investigaciones Científicas y Técnicas de Argentina, 1650 Buenos Aires, Argentina; †Laboratorio de Mecanismos Moleculares de Carcinogénesis, Instituto de Biología y Medicina Experimental, Consejo Nacional de Investigaciones Científicas y Técnicas de Argentina, 1428 Buenos Aires, Argentina; ‡Instituto de Medicina Experimental, Consejo Nacional de Investigaciones Científicas y Técnicas de Argentina, Academia Nacional de Medicina, 1425 Buenos Aires, Argentina; §Fundación Instituto Leloir, Instituto de Investigaciones Bioquímicas de Buenos Aires, Consejo Nacional de Investigaciones Científicas y Técnicas de Argentina, 1405 Buenos Aires, Argentina; and ¶Instituto de Inmunología, Genética y Metabolismo, Laboratorio de Inmunogenética, Hospital de Clínicas "José de San Martín," Consejo Nacional de Investigaciones Científicas y Técnicas de Argentina, Universidad de Buenos Aires, 1120 Buenos Aires, Argentina

ORCIDs: 0000-0002-9220-2210 (F.S.); 0000-0001-6944-7896 (P.M.B.); 0000-0002-7776-3378 (R.S.); 0000-0001-7254-1082 (A.S.T.); 0000-0003-4448-0977 (K.A.P.).

Received for publication May 26, 2015. Accepted for publication March 15, 2016.

This work was supported by grants from the Bill & Melinda Gates Foundation through the Grand Challenges Explorations Initiative (Phase I, Grants OPP1017298 and OPP1060394; Phase II, Grant OPP1119024), by Agencia Nacional de Promoción Científica y Tecnológica (Argentina) Grants PICT 2010-1163 and PICT 2006-1670, and by Agencia Nacional de Promoción Científica y Tecnológica (Argentina)/Conselho Nacional de Pesquisas Grant PICT 2008-18 (to J.C.). The funders had no role in experimental design, data collection and analysis, decision to publish, or preparation of the manuscript.

Address correspondence and reprint requests to Dr. Juliana Cassataro, Instituto de Investigaciones Biotecnológicas "Dr. Rodolfo A. Ugalde," IIB-INTECH, UNSAM-CONICET, Avenida 25 de Mayo y Francia, 1650 San Martín, Buenos Aires, Argentina. E-mail address: jucassataro@iibintech.com.ar

The online version of this article contains supplemental material.

Abbreviations used in this article: BM, bone marrow; BMDC, BM-derived DC; BMDM, BM-derived macrophage; DC, dendritic cell; DLN, draining lymph node; K_i, inhibition constant; K_m, Michaelis constant; K_m^{app}, the apparent value of Michaelis constant at different inhibitor concentrations; MHC I, MHC class I; MHC II, MHC class II; Omp, outer membrane protein; PK, proteinase K; ROI, region of interest; [S], substrate concentration; U, unlipidated; [U-Omp19], unlipidated Omp19 (inhibitor) concentration; UNSAM, University of San Martin; V_0, initial velocity; V_{max}, maximum velocity; V_{max}^{app}, apparent value of maximum velocity at different inhibitor concentrations; YG, yellow green.

Our group has been working on the use of the protein moiety of the lipoprotein outer membrane protein (Omp)19 from *Brucella abortus* (unlipidated [U]-Omp19) as a vaccine candidate against *Brucella* (19, 20). We have demonstrated that U-Omp19 is a protein with self-adjuvanting capacity, because oral or systemic immunization with U-Omp19 (produced either in *Escherichia coli* or in plants) without adjuvants conferred significant protection against oral or systemic *B. abortus* infection and induced a Th 1 response independent of TLR4. U-Omp19 also induced the maturation of murine DCs in vivo (20) and increased Th1 immune responses to coadministered Ags (21). Sequence analysis of U-Omp19 has revealed a significant sequence identity with other bacterial protease inhibitors, particularly with inh from *Erwinia chrysanthemi* (family I38). This family of proteins interacts with specific proteases released by plant, insect, and animal pathogens (22, 23). We have recently demonstrated that U-Omp19 inhibits main gastrointestinal proteases protecting codelivered Ags in oral vaccines from digestion and increases immune responses (24). As there are known protease inhibitors that could inhibit serine and also cysteine proteases (23), in this work we evaluated whether the *Brucella* spp. protease inhibitor U-Omp19 can limit lysosomal proteolytic capacity of APCs.

Despite the notion and extensive literature indicating that limiting the proteolytic capacity of APCs can increase Ag immunogenicity, to our knowledge there are no published reports describing successful in vivo vaccine intervention/immunization (increased immune responses) using this concept. Although blocking Ag proteolysis by potent protease inhibitors may impair immunogenicity, partial inhibition of lysosomal proteases may increase Ag half-life within lysosomes and result in an increased Ag immunogenicity. We demonstrated that the s.c. codelivery of U-Omp19 with the Ag 1) reduces the susceptibility of the Ag to intracellular proteolysis in DCs, 2) extends Ag intracellular half-life, and 3) increases Ag cross-presentation and Ag-specific $CD8^+$ T cell responses in vivo.

Materials and Methods

Ethics statement

All experimental protocols with animals were conducted in strict accordance with international ethical standards for animal experimentation (Declaration of Helsinki and its amendments, Amsterdam protocol of welfare and animal protection, and National Institutes of Health *Guide for the Care and Use of Laboratory Animals*). The protocols of this work were also approved by the Institutional Committee for the Care and Use of Laboratory Animals from the University of Buenos Aires and from the University of San Martin (Buenos Aires, Argentina).

Animals

Eight-week-old female BALB/c and C57BL/6 mice were purchased from University of La Plata (La Plata, Argentina) or from University of San Martin (UNSAM) and housed in the animal resources facility of the University of Buenos Aires or UNSAM (Buenos Aires, Argentina). OT-I/RAG1 (OT-I) mice were obtained from The Jackson Laboratory and were bred in the animal facility of UNSAM or Leloir Institute. GFP C57BL/6 mice were bred in the animal facility of UNSAM.

Ags and adjuvants

Chicken egg OVA grade V (Sigma-Aldrich) was used as model Ag. Recombinant U-Omp19 was obtained as previously described (19). LPS contamination from OVA and U-Omp19 were adsorbed with sepharose–polymyxin B (Sigma). Endotoxin determination was performed with a *Limulus* amebocyte chromogenic assay (Lonza). In some experiments U-Omp19 fully digested with proteinase K (PK) was used as a control. U-Omp19 was treated with PK-agarose from *Tritirachium album* (Sigma-Aldrich) for 1 h at 37˚C. The enzyme immobilized in agarose was then centrifuged out and the supernatants were incubated for 2 h at 60˚C to inactivate any fraction of soluble enzyme. The complete digestion of U-Omp19 was checked by SDS-PAGE. All U-Omp19 and OVA preparations used contained <0.1 endotoxin units per milligram protein. Aprotinin, leupeptin, recombinant human cystatin C expressed in HEK293 cells, IFA, and CFA were purchased from Sigma-Aldrich. Unless specified otherwise, protease inhibitors were used in the following concentrations: U-Omp19, 100 μg/ml (6.25 μM); aprotinin, 1 μg/ml (0.15 μM); leupeptin, 5 μg/ml (10 μM); and cystatin, 6.5 μg/ml (0.5 μM).

Determination of protease inhibitor activity in vitro

The protease activity was measured as the increase of BODIPY FL fluorescence released from cleaved BODIPY FL–labeled casein using the EnzChek protease assay kit (Molecular Probes). The increase in fluorescence emission is proportional to casein digestion and protease activity. Cathepsin L (0.088 μM, Sigma-Aldrich), C (0.014 μM, Sigma-Aldrich), B (3.6 μM, Sigma-Aldrich), and papain (0.965 μM, Sigma-Aldrich) were incubated with U-Omp19 at different protease/U-Omp19 molar ratios (1:1, 1:5, 1:8, and 1:10). As positive control, a mammalian protease inhibitor mixture (Sigma-Aldrich) was used. U-Omp16,a *Brucella* spp. protein with a similar molecular mass to U-Omp19 and expressed and purified in the same way, was used as negative control. Known protease inhibitors (leupeptin or cystatin C) were also used as controls. Each reaction mix was incubated at room temperature for 1 h and then 1 μg/ml substrate (casein–BODIPY FL) was added. Fluorescence emission was measured with a fluorescence plate reader (FilterMax F5, Molecular Devices).

Kinetic assay

Cathepsin L activity assays were performed in 400 mM sodium acetate, 4 mM EDTA (pH 5), and 8 mM DTT. For inhibition assays, recombinant purified U-Omp19 was incubated at different concentrations with human cathepsin L (0.25 nM). Proteolytic activity was then analyzed by measuring the hydrolysis of different amounts of the specific fluorogenic substrate Ac-HRYR-ACC (Calbiochem, San Diego, CA). Fluorescence release was measured using a Beckman Coulter DTX 880 microplate fluorimeter with 360- (excitation) and 450-nm (emission) filters and Multimode detection software. Data were analyzed using Prism 5.0 (GraphPad Software). Linear regressions of fluorescence units versus time (seconds) were used to calculate initial velocities (V_0) for each substrate concentration [S] and inhibitor concentration [U-Omp19] combination sample. Data were plotted in terms of V_0 as a function of [S] for each [U-Omp19] and fitted to the Michaelis–Menten equation using GraphPad Prism 5.0 software to determine the values of K_m^{app} (i.e., the apparent value of Michaelis constant [K_m] at different inhibitor concentrations) and V_{max}^{app} (i.e., the apparent value of maximum velocity [V_{max}] at different inhibitor concentrations) directly from the nonlinear least-squares best fits of the untransformed data. Data were transformed into Lineweaver–Burk plots ($1/V_0$ versus 1/[S]). For Lineweaver–Burk plots, the determined values of $-1/K_m^{app}$ for $1/V_0 = 0$ and $1/V_{max}^{app}$ for 1/[S] = 0 were also plotted. Best fit lines were generated by linear regression analysis. These plots were used in the assessment of the type of mechanism of inhibition (25, 26). Global nonlinear fits of untransformed data were used to calculate the inhibition constant (K_i) value using GraphPad Prism 5.0 software following a model of competitive mechanism of inhibition.

Bone marrow–derived DCs and bone marrow–derived macrophages

DCs and macrophages were generated from bone marrow (BM) mononuclear cells from wild-type C57BL/6 or GFP mice. Briefly, femurs and tibiae were collected from 6- to 12-wk-old mice. After removing bone-adjacent muscles, marrow cells were extracted by flushing RPMI 1640 medium through the bone interior. BM cells were then suspended on DC culture medium (RPMI 1640 medium, 10% heat-inactivated fetal/bovine serum, 1 mM sodium pyruvate, 2 mM L-glutamine, 100 U penicillin/ml, 100 mg streptomycin/ml, 50 mM 2-ME, and 20 ng/ml GM-CSF) or monocyte culture medium (RPMI 1640 medium, 10% heat-inactivated fetal/bovine serum, 1 mM sodium pyruvate, 2 mM L-glutamine, 100 U penicillin/ml, 100 mg streptomycin/ml, and 20 ng/ml M-CSF) and plated on six-well plates (1.5×10^6 cells/2 ml culture medium). On days 3 and 5, the cells were refed. On day 8, cells were harvested and the expression of DC ($CD11c^+$, MHC class II [$MHC\ II]^{low}$) or monocyte (F4/80) markers was analyzed by flow cytometry using FACSAria II flow cytometer (BD Biosciences) with FACSDiva software (BD Biosciences) and further analyzed using FlowJo 7.5 software (Tree Star).

APC microsome protease activity assay

Microsomes from BM-derived DCs (BMDCs) and BM-derived macrophages (BMDMs) were obtained as previously described (10). Fifty or 100 μg microsomes were incubated alone or with different amounts of U-Omp19 (1, 10, 50, or 100 μg) for 1 h. As positive control, a protease inhibitor mixture (Sigma-Aldrich) was used. U-Omp16 (100 μg) was used

as negative control. Then, casein BODIPY substrate (1 μg) was added to the samples. Fluorescence emission was measured with a fluorescence plate reader (Victor^3, PerkinElmer, Waltham, MA).

Determination of protease inhibitor activity in APCs

To study protease inhibitor activity in BMDCs and BMDMs in vitro, 5×10^5 cells were incubated during 1 h with casein BODIPY or OVADQ (Molecular Probes) alone or with U-Omp19. Leupeptin and BSA were used as positive and negative controls, respectively. Casein or OVA degradation was measured in living cells by flow cytometry using a FACSAria II flow cytometer with FACSDiva software and further analyzed using FlowJo 7.5 software.

Determination of cathepsin L protease activity in live APCs

To study specific cathepsin L activity in live BMDCs and BMDMs, cells (5×10^5 cells/ml) were incubated with OVA alone or with U-Omp19 in HBSS medium during 60 min. Leupeptin and BSA were used as controls. After incubation, cells were washed and incubated with cell-permeant quenched fluorogenic substrate specific for cathepsin L $(CBZ\text{-}Phe\text{-}Arg)_2$ (Invitrogen) for different periods of time at 37°C. Cells were then washed and counted with trypan blue. The fluorescence emission of cells was measured with a fluorescence plate reader or by flow cytometer.

Confocal laser scanner microscopy analysis of cathepsin L inhibition by U-Omp19, leupeptin, and cystatin C was evaluated in live cells. BMDCs (2×10^5 cells) were plated in glass chambers slides and then treated with medium alone, U-Omp19, leupeptin, or cystatin C for 30 min. Then, BMDCs were washed and incubated with LysoTracker dye (Invitrogen) plus the fluorogenic cathepsin L substrate (Invitrogen) for 30 min. Images were acquired with an IX81 microscope with a confocal FV1000 module and a PLAN APO ×60 (numerical aperture 1.42) oil immersion objective (Olympus), and the acquisition software used was FV10-ASW 3.1. For colocalization quantification of LysoTracker/cathepsin L substrate, the Coloc 2 plugin in ImageJ software (National Institutes of Health) was used and the Manders' coefficient was calculated. Single regions of interest (ROI; LysoTracker positive compartments) were determined automatically with Analyze Particle plugin and the Manders' colocalization coefficient was measured in each ROI.

Internalization in vitro

BMDCs (1×10^6 cells/ml) were incubated with protein Ags, including OVA–Alexa Fluor 647 (Invitrogen) and GFP, or with nonprotein Ags, including dextran–Alexa Fluor 647 (Invitrogen) and yellow green (YG) microspheres (Polysciences Fluoresbrite microparticles, 1.024 μm), in presence of complete medium or U-Omp19 during 30 or 60 min. Leupeptin, cystatin C, and BSA were used as positive and negative controls, respectively. Then, cells were washed and the presence of Ag within cells was determined by flow cytometry. In some experiments, BMDCs were pretreated with LPS (100 ng/ml) for 12 h and then incubated with the protein Ag OVA–Alexa Fluor 488 (Invitrogen) or nonprotein Ags, including dextran-FITC (Sigma-Aldrich) and YG microspheres (Polysciences Fluoresbrite microparticles, 1.024 μm).

Recruitment of APCs in vivo

Animals were s.c. administered once with OVA (50 μg) plus buffer, U-Omp19 (100 μg), or aprotinin (1 μg). Draining lymph nodes (DLNs) were obtained 18 h later and single-cell suspensions were prepared. Total viable cells were counted using trypan blue. Cells were stained with fluorochrome-conjugated Abs, including anti-CD11c, anti–MHC II, anti-CD11b, anti-CD8α, or isotype-matched controls, for 30 min at 4°C. Afterward, cells were washed and analyzed by flow cytometry analysis. mAbs were purchased from eBioscience (San Diego, CA), BioLegend (San Diego, CA), and BD Biosciences (Franklin Lakes, NJ). In other experiments, mice were s.c. administered with dextran-FITC (200 μg) or dextran-FITC plus U-Omp19 (100 μg) and 18 h later DLNs were obtained and cell suspensions were prepared. Cells were stained with a viability dye (Zombie Aqua, BioLegend) followed by staining with fluorochrome-conjugated Abs, including anti-CD11c, anti–MHC II, anti-CD11b, anti-CD8α, anti-CD103, anti-CD207, anti-LyC, or anti-Ly6G, for 30 min at 4°C. Afterward, cells washed and analyzed by flow cytometry.

Migration of DCs in vivo

BMDCs were obtained from GFP mice and pulsed with medium alone, U-Omp19 (100 μg/ml), or LPS (100 ng/ml) for 18 h and then 5×10^6 cells were s.c. injected to wild-type recipient mice as described in Toki et al. (27). After 12 h, DLNs were obtained and the presence of migratory GFP^+ cells was analyzed by flow cytometry.

Determination of Ag fate and degradation in vivo

BALB/c mice (n = 3/group) were s.c. administered with OVADQ and OVA–Alexa Fluor 647 (25 μg each Ag) simultaneously plus buffer, U-Omp19 (100 μg), or aprotinin (1 μg). Spleen and DLNs were removed 12 h afterward and cell suspensions were obtained. Total viable cells were counted using trypan blue. Cells were stained with fluorochrome-conjugated Abs, including anti-CD11c, anti-CD11b, anti-CD8α, or isotype-matched controls, for 30 min at 4°C. Cells were then washed and Ag presence and digestion were determined in the different cell populations by flow cytometry.

Studying Ag fate inside DCs by confocal microscopy

BMDCs (2×10^5 cells) were plated in chamber slides (Nunc) and incubated for 30 or 60 min with OVA–Alexa Fluor 647 (50 μg/ml) alone or with U-Omp19 (100 μg/ml) in RPMI 1640 complete medium. After incubation, cells were washed with saline and fixed with 2% paraformaldehyde for 15 min. Then, cells were permeabilized with 0.2% saponin for 30 min and stained with anti-Omp19 polyclonal serum obtained from rabbit (dilution 1:2000) and anti–Lamp-2 (1:500; BD Biosciences). As secondary Abs, anti-rabbit IgG–Alexa Fluor 488 or anti-mouse Ig–Alexa Fluor 546 (Invitrogen) were used. Then, slides were mounted with Aqua-Poly/Mount (Polysciences) and were analyzed using an IX-81 microscope attached with a FV-1000 confocal module at 23°C. For colocalization quantification of Lamp-2/OVA, the Coloc 2 plugin in ImageJ software was used and the Manders' coefficient was calculated. Single ROIs ($Lamp\text{-}2^+$ compartments) were determined automatically with Analyze Particle plugin and the Manders' colocalization coefficient was measured in each ROI.

Determination of MHC I/OVA peptide complexes

BMDCs (1×10^6 cells/ml) were incubated with OVA (50 μg/ml) alone or plus U-Omp19 (100 μg/ml) or U-Omp19 (100 μg/ml) plus MG132 proteasomal inhibitor during 3 h at 37°C. Then, cells were washed and incubated at different times (0, 2, 6, 12, and 18 h). Expression of $H\text{-}2K^b/OVA_{257–264}$ complexes in the surface of DCs was evaluated by labeling the cells with the specific mAb 25D1.16 anti-OVA–derived peptide SIINFEKL bound to $H\text{-}2K^b$ of MHC I (eBioscience). Samples were analyzed by flow cytometry.

In vitro cross-presentation assay

BMDCs ($CD11c^+MHC\ II^{low}$) from C57BL/6 mice (1×10^6) were pulsed with complete medium, OVA (50 μg/ml), OVA plus U-Omp19 (100 μg/ml), or OVA plus U-Omp19 digested with PK (100 μg/ml) for 24 h. Then, DCs were washed and cocultured with OT-I Thy1.1 cells (2×10^6 cells) at 37°C. Anti-CD107a or isotype-matched control Ab was added during the last 6 h of stimulation. During the last 5 h, cells were treated with brefeldin A and monensin. Afterward, cells were washed and stained with anti-CD8 and anti-CD62L and then fixed, permeabilized with saponin, and stained with anti–IFN-γ or isotype-matched control. Production of intracellular IFN-γ by $CD8^+$ T cells, downregulation of CD62L, and degranulation by expression of CD107a were assessed by flow cytometry. Similar experiments were performed with GFP OT-I chimera protein as Ag and including leupeptin and aprotinin stimulation (28). In other experiments, BMDCs were pulsed with medium, OVA, OVA plus U-Omp19, OVA plus leupeptin, or OVA plus cystatin C in the presence or absence of LPS (100 ng/ml). Cross-presentation to OT-I cells by DCs was assessed as described above.

Adoptive transfer of OT-I cells and in vivo $CD8^+$ T cell proliferation

Single-cell suspensions of spleen and DLNs cells from OT-I mice were labeled with 5 μM CFSE (Molecular Probes) prior to i.v. injection. One day before immunization, 10×10^6 OT-I cells were injected i.v. in C57BL/6 sex-matched recipients. Transferred mice received a single s.c. dose of OVA (30 μg) plus U-Omp19 (100 μg), PK-digested U-Omp19 (100 μg), LPS (1 μg), or saline. In other experiments, transferred mice were s.c immunized with OVA (30 μg) alone or with protease inhibitors, including U-Omp19 (100 μg), leupeptin (5 μg), or cystatin C (6.5 μg). Five days after immunization, mice were sacrificed and spleen and DLN suspensions were obtained to study the proliferation of $CD8^+$ T cells by flow cytometry.

Intracellular IFN-γ determination

C57BL/6 mice were immunized s.c. on days 0, 7, and 14 with saline, OVA (60 μg), OVA plus U-Omp19 (100 μg), OVA + CFA (first dose), or IFA (second and third doses). Three weeks after the last immunization, mice were sacrificed to study cellular immune response. Spleen cells were cultured (4×10^6 cells/well) in the presence of complete medium

(supplemented with IL-2) or Ag stimuli (IL-2 plus OVA [500 μg/ml], B16-OVA [MO5 cells] mitomycin-treated cells as a source of APCs [25:1], and $OVA_{257–264}$ peptide [5 μg/ml]) for 18 h. Next, brefeldin A was added for 5 h more to the samples. After that, cells were washed, fixed, permeabilized, stained, and analyzed by flow cytometry.

Tumor experiments

C57BL/6 mice (n = 6/group) were immunized s.c. on days 0, 7, and 14 with OVA, OVA plus U-Omp19, or OVA plus CFA/IFA. Three weeks later, immunized mice were injected s.c. in the right flank with 1×10^5 MO5 cells (B16 murine melanoma cells expressing OVA). Animals were monitored and tumor growth was measured three times a week as described previously (29).

Statistical analysis

Statistical analysis and plotting were performed using GraphPad Prism 5 software (GraphPad Software, San Diego, CA). In experiments with more than two groups, data were analyzed using one-way ANOVA with a Bonferroni posttest. In the experiment of MHC I/OVA complex expression, data were analyzed using two-way ANOVA with a Bonferroni posttest. When necessary, a logarithmic transformation was applied prior to the analysis to obtain data with a normal distribution. In experiments with two groups, an unpaired t test or Mann–Whitney U test were used. A p value <0.05 was considered significant. When bars are plotted, results are expressed as means ± SEM for each group. In survival experiments, Kaplan–Meier curves were generated by using GraphPad Prism 5 software and analyzed with a log-rank test.

Results

U-Omp19 is a lysosomal protease inhibitor

The capacity of U-Omp19 to limit the activity of cysteine proteases was first examined. U-Omp19 partially inhibited the activity of proteases in vitro (cathepsin L, C, and B and papain) ($p < 0.05$, $p < 0.01$, or $p < 0.001$ versus no inhibitor). U-Omp16, a recombinant protein from *Brucella* obtained using a similar method to U-Omp19, caused no effect when used in similar molar ratios to U-Omp19, whereas a commercial protease inhibitor mixture inhibited all proteases (Fig. 1A). Besides the capacity of U-Omp19 to inhibit purified proteases, it also inhibited the digestive capacity of microsomal content obtained from BMDCs and BMDMs ($p < 0.05$, $p < 0.01$, or $p < 0.001$ versus no inhibitor). As expected, U-Omp16 had no inhibitory effect whereas a protease inhibitor mixture reduced the proteolytic function of microsomes (Fig. 1B, 1C). Collectively, these results indicate that U-Omp19 is a cysteine protease inhibitor and it can inhibit lysosomal proteases from APCs in vitro.

U-Omp19 is a competitive inhibitor of cathepsin L

To study the inhibition mechanism of U-Omp19, kinetics studies of the hydrolysis of a specific fluorogenic substrate (Ac-HRYR-ACC) were performed in the presence of increasing concentrations of U-Omp19. Progress curves for substrate hydrolysis at different initial substrate and U-Omp19 concentrations were used to obtain V_0. Kinetic data were fit to a Michaelis–Menten model (Fig. 1D), and a nonlinear regression was conducted to obtain K_m^{app} and V_{max}^{app} values. GraphPad software was used to fit experimental data to different models of inhibition mechanisms. Several inhibition mechanisms, including competitive, uncompetitive, noncompetitive, and mixed noncompetitive, were tested independently. Comparison of models based on parameter errors, fitting accuracy, and model discrimination analysis within the GraphPad software consistently highlighted the competitive inhibition model as the best model to replicate the kinetic data ($r^2 = 0.932$) with a K_i of 2 ± 0.44 (μM). Moreover, the Lineweaver–Burk plot was compatible with a typical first-order competitive inhibitor (Fig. 1E). Therefore, these results indicate that U-Omp19 is a competitive inhibitor of cathepsin L with a K_i in the micromolar range.

U-Omp19 has lysosomal protease inhibitor activity within live APCs

To determine the inhibitor capacity of U-Omp19 in living cells, OVADQ or casein BODIPY, which fluoresces only after degradation, as model Ags were used to trace their intracellular proteolysis. Thus, bone marrow–derived APCs were incubated with Ag alone or plus U-Omp19 and Ag digestion was evaluated by flow cytometry. Leupeptin was used as positive control and BSA as negative control of this assay. U-Omp19 or leupeptin codelivered with OVADQ or casein BODIPY significantly reduced Ag degradation by DCs and macrophages ($p < 0.01$ or $p < 0.001$ versus no inhibitor) whereas BSA did not (Fig. 2A, 2B).

Next, the ability of U-Omp19 to inhibit the activity of cathepsin L inside live cells was evaluated. To conduct this, DCs or macrophages were incubated with OVA, OVA plus U-Omp19, or OVA plus leupeptin and then pulsed with a cell-permeable cathepsin L–specific fluorogenic substrate $(CBZ\text{-}Phe\text{-}Arg)_2$ that fluoresces upon digestion. Live cells pulsed with U-Omp19 or leupeptin showed a partial reduction in the enzyme activity inside both DCs and macrophages at different time points after incubation (Fig. 2C, 2D, $p < 0.05$ and $p < 0.001$ versus OVA). Cathepsin L activity inhibition was also evaluated by confocal microscopy. DCs were incubated with U-Omp19, leupeptin, or cystatin C for 30 min and then washed and labeled with LysoTracker Red DND-99 dye. LysoTracker is a cell-permeant dye that accumulates and fluoresces in acidic compartments in live cells. Simultaneously with LysoTracker, cells were incubated with the quenched fluorogenic substrate of cathepsin L for 30 min. Colocalization of the digested substrate (fluorescent, green) and LysoTracker (red) was evaluated by a Manders' coefficient in living cells. Results indicated that U-Omp19, leupeptin, and cystatin C induced a decrease in the colocalization of LysoTracker (lysosomes) with the digested cathepsin L substrate compared with the incubation of DCs with medium alone (Fig. 2E, 2F, $p < 0.01$, $p < 0.05$, or $p < 0.01$ versus medium). These results indicate that U-Omp19 partially inhibits lysosomal cathepsin L activity inside live DCs.

There were no changes in the activation status or in the expression levels of cathepsins upon incubation of APCs with U-Omp19 as studied by Western blot (Supplemental Fig. 1A). Furthermore, there were no changes in the intracellular pH of BMDCs and BMDMs after 1 h of incubation with U-Omp19, indicating that this protein does not affect proteases maturation (Supplemental Fig. 1B). Of note, U-Omp19, leupeptin, and cystatin C inhibited cathepsin L activity inside live LPS-treated DCs measured by two different methods: fluorimetry (Supplemental Fig. 1C) and flow cytometry (Supplemental Fig. 1D). Because U-Omp19 is able to activate DCs (20), this result indicates that the observed inhibition of U-Omp19 is not an indirect consequence of changes undertaken by DCs during maturation (30).

Collectively, these results indicate that U-Omp19 can limit proteolytic activity inside live APCs.

U-Omp19 increases the amount of Ag inside APCs

Limiting Ag degradation by lysosomal proteases inside APCs would increase Ag intracellular half-life (11). Thus, the amount of internalized Ags by APCs (protein Ags, OVA–Alexa Fluor 647 and GFP; nonprotein Ags, dextran-FITC and YG microspheres) was evaluated at different time points after coincubation with buffer, U-Omp19, leupeptin, or BSA. At 30 min after coincubation, there were no significant differences in the amount of internalized Ag among treated groups (Fig. 3). However, a larger amount of OVA–Alexa Fluor and GFP was found in BMDCs after 60 min of coincubation with U-Omp19 (Fig. 3A, 3B, $p < 0.05$ and $p < 0.001$ versus Ag alone) compared with the protein alone (OVA

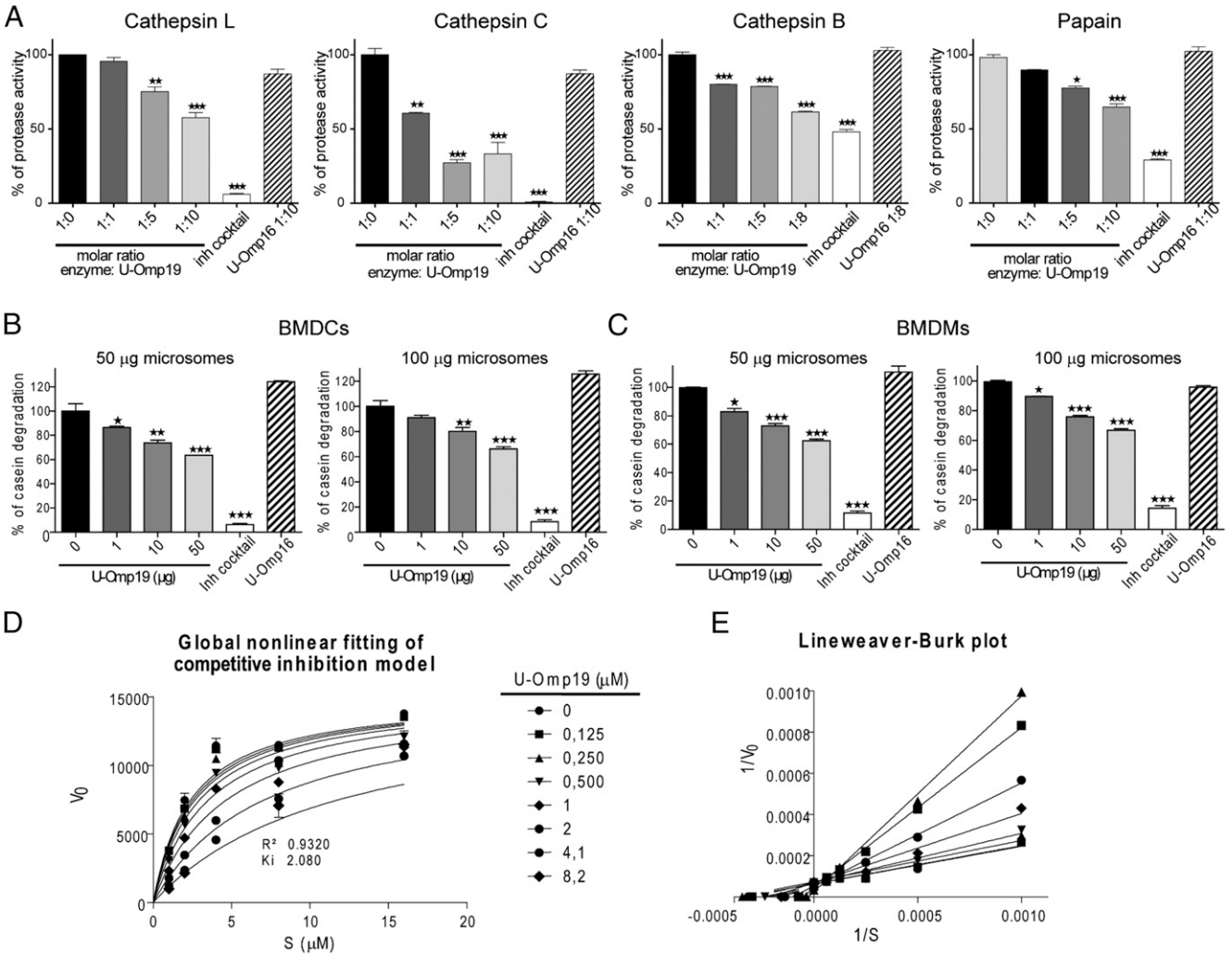

FIGURE 1. U-Omp19 is a cysteine protease inhibitor. (**A**) Protease inhibitor activity was determined using a casein BODIPY FL assay kit. Cathepsin L, C, B, and papain were preincubated in the optimal buffer for each enzyme for 1 h at different molar ratios with U-Omp19 (enzyme: U-Omp19, 1:1, 1:5, 1:8, and 1:10) or without U-Omp19 (1:0). A mammalian protease inhibitor mixture was used as a positive control and U-Omp16 as a negative control at a 1:8 or 1:10 molar ratio. Then, 1 μg/ml casein BODIPY FL was added and the emission of fluorescence was evaluated. Inhibitor activity is expressed as percentage of protease activity remaining compared with condition 1:0 ($^{\star}p < 0.05$, $^{\star\star}p < 0.01$, $^{\star\star\star}p < 0.001$ versus 1:0 condition). Protease inhibitor activity on microsomes from BMDCs (**B**) or BMDMs (**C**) was determined using a casein BODIPY FL assay kit. Microsomes (50 or 100 μg) were incubated with different amounts of U-Omp19 (1, 10, or 50 μg) for 1 h. A mammalian protease inhibitor mixture was used as positive control and U-Omp16 as negative control. Inhibitor activity is expressed as percentage of casein degradation ($^{\star}p < 0.05$, $^{\star\star}p < 0.01$, $^{\star\star\star}p < 0.001$ versus without U-Omp19). The inhibition mechanism of U-Omp19 on cathepsin L was evaluated using a specific substrate. Different concentrations of U-Omp19 were incubated with cathepsin L before addition of the indicated specific substrate concentrations. Proteolytic activity was measured as the increment in fluorescence units of samples. Linear regressions of fluorescence units versus time (seconds) were used to calculate V_0 for each [S] and [U-Omp19] combination sample (**D**). Global nonlinear fits of data were used to calculate K_i value. Data were transformed into Lineweaver–Burk plots ($1/V_0$ versus 1/[S]) (**E**). Each panel is representative of three independent experiments.

or GFP). Leupeptin codelivery induced an increase in OVA inside DCs at 60 min ($p < 0.01$ versus OVA alone). In contrast, even at 30 or 60 min after incubation there were no significant increases in the amount of nonprotein Ags (Fig. 3C, 3D). Next, and to ensure equal Ag uptake in all samples, DCs were incubated for 60 min with LPS, washed, and then the Ag (OVA–Alexa Fluor 488, dextran-FITC, or YG particles) was chased in the presence of U-Omp19, leupeptin, cystatin C, or BSA. BMDCs incubated with U-Omp19, leupeptin, or cystatin C showed a larger amount of OVA–Alexa Fluor after 60 min (Supplemental Fig. 2A, $p < 0.05$ versus Ag alone) compared with OVA alone. However, there was not a significant increment in the amount of dextran-FITC or YG particles after incubation with the inhibitors at any time assayed (Supplemental Fig. 2B, 2C).

These results demonstrate that U-Omp19 increases the amount of the coadministered Ag inside APCs but does not increase endocytosis (pinocytosis or phagocytosis). They also indicate that the observed increase in the amount of protein Ag inside DCs when U-Omp19 is codelivered is not a consequence of DC maturation and is due to inhibition of Ag intracellular proteolysis (31).

U-Omp19 induces APC recruitment to DLNs and reduces Ag degradation inside APCs after its coadministration in vivo

To induce an adaptive immune response, Ag-bearing APCs must reach lymph nodes where immunological synapse takes place. To evaluate recruitment of APCs and Ag proteolysis and amount in vivo, BALB/c mice were s.c. inoculated with OVA alone or with U-Omp19 or aprotinin as control. Twelve hours later, lymph nodes and spleens were obtained and cell populations were evaluated. There was a significant increment in the recruitment of $CD8\alpha^+$ DCs ($CD11c^+CD11b^-CD8\alpha^+$, $p < 0.01$ versus OVA) and monocytes

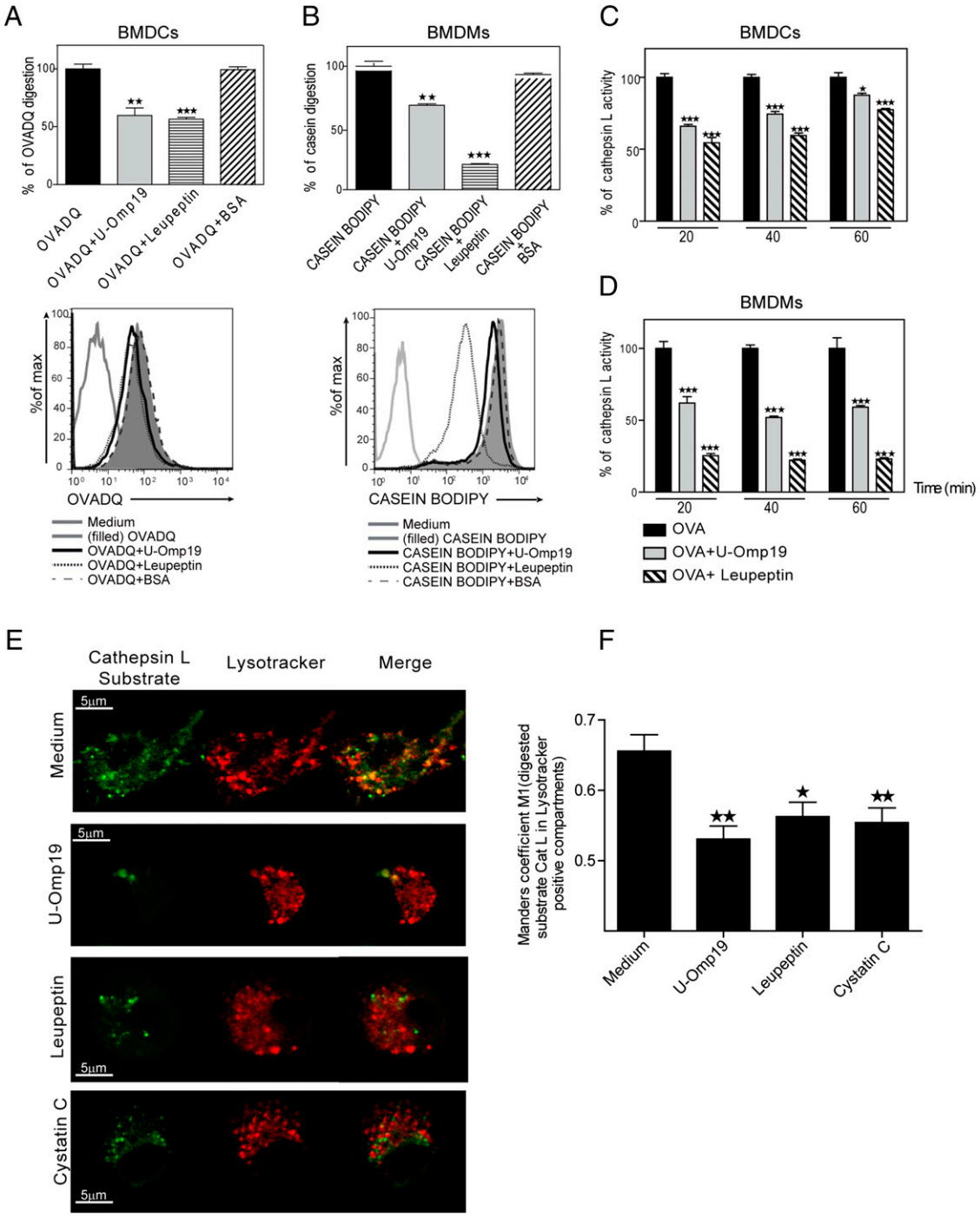

FIGURE 2. U-Omp19 inhibits lysosomal proteases in live DCs. Protease inhibitor activity on BMDCs (**A**) or BMDMs (**B**) was determined by flow cytometry using casein BODIPY or OVADQ. Cells were incubated for 1 h in the presence of U-Omp19 or controls (leupeptin or BSA) Inhibitor activity is expressed as percentage of OVA or casein digestion; overlaid histograms represent Ag fluorescence intensity of each group ($^{**}p < 0.01$, $^{***}p < 0.001$ versus casein or OVA alone). Specific U-Omp19 inhibitor activity on cathepsin L was evaluated in BMDCs (**C**) or BMDMs (**D**). Cells were incubated with OVA alone or plus U-Omp19 or leupeptin for 1 h. Then, a fluorogenic cathepsin L substrate was added for different periods of time and the fluorescence emission was evaluated. Inhibitor activity is expressed as percentage of cathepsin L activity ($^{*}p < 0.05$, $^{***}p < 0.001$ versus OVA alone). Confocal laser scanning microscopy analysis of cathepsin L inhibition activity by U-Omp19, leupeptin, and cystatin C in live DCs is shown (**E**). BMDCs were treated with medium alone, U-Omp19, leupeptin, or cystatin C and then washed and incubated with LysoTracker (red) and the fluorogenic cathepsin L substrate (green). Images are representative of most cells examined by confocal microscopy. LysoTracker colocalization with cathepsin L substrate was quantified by a Manders' coefficient (M1) (**F**). High Manders' coefficients indicate better colocalization. Data are means of Manders' coefficients ± SEM from at least 200 regions of interest (lysosomes) from five images analyzed of each condition. Results are representative of two independent experiments ($^{*}p < 0.05$, $^{**}p < 0.01$ versus medium).

($CD11b^{+}CD11c^{-}$MHC $II^{+}CD8^{-}$, $p < 0.05$ versus OVA) to DLNs but not to spleen when U-Omp19 was codelivered with OVA. In contrast, aprotinin did not increase recruitment of APCs (Fig. 4A).

Cell subset recruitment to lymph nodes after s.c. administration of U-Omp19 was further characterized by incorporating a fluorescent cell tracker (dextran-FITC) and CD11c, CD11b, MHC II,

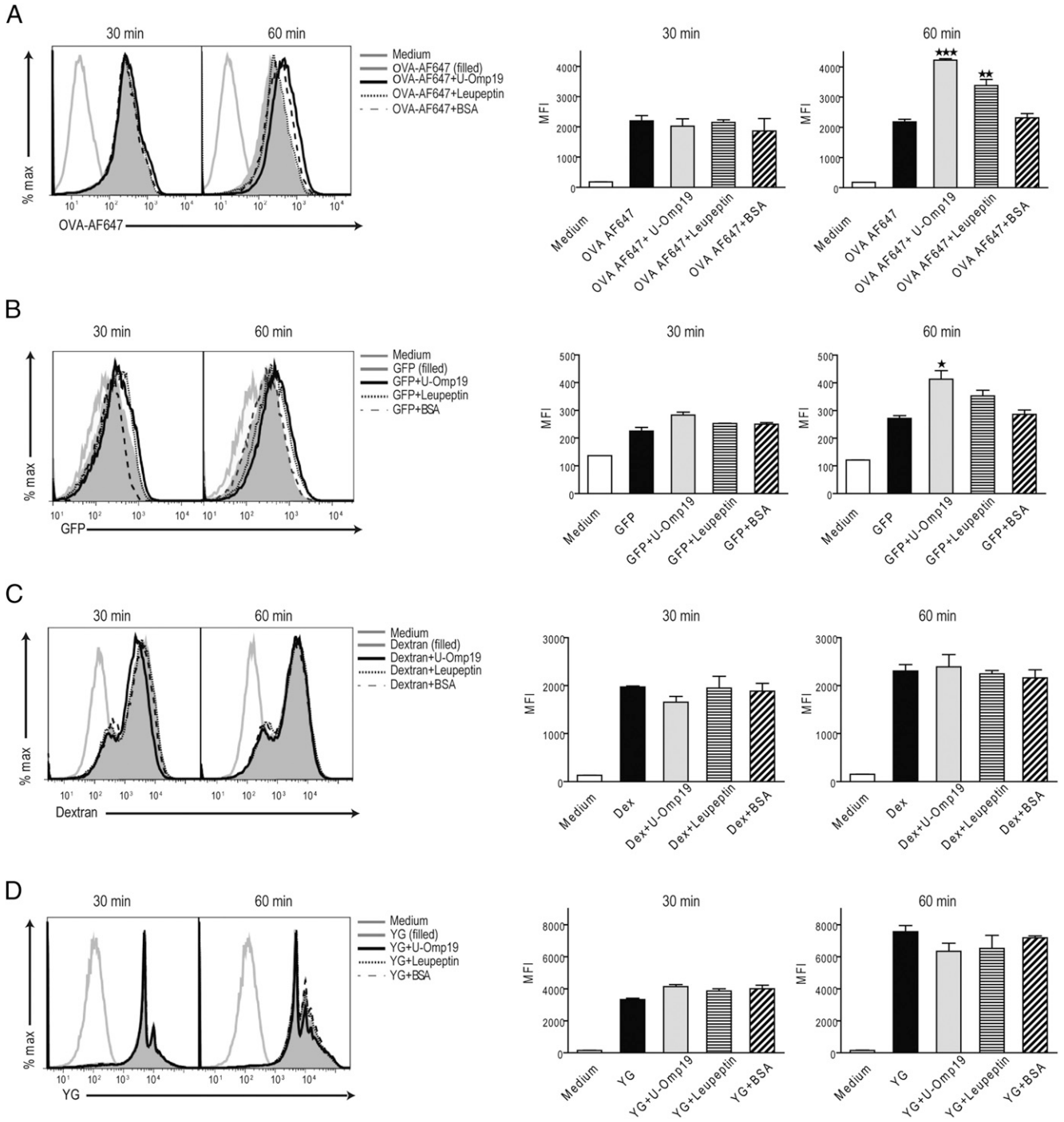

FIGURE 3. U-Omp19 increases the amount of Ag inside DCs. DCs were incubated during 30 or 60 min with OVA–Alexa Fluor 647 (**A**), GFP (**B**), dextran-FITC (**C**), or YG microspheres (**D**) alone or plus U-Omp19, leupeptin, or BSA. Then, cells were washed and fluorescence emission was evaluated by flow cytometry. Results are shown as representative histograms and as the mean fluorescence intensity (MFI) ± SEM for each group and are representative of three different experiments ($^{\star}p < 0.05$, $^{\star\star}p < 0.01$, $^{\star\star\star}p < 0.001$ versus Ag alone).

CD8α, CD103, and CD207 (Langerin) markers. Subcutaneous injection of U-Omp19 increased the recruitment of dextran-FITC$^+$ DCs (dextran-FITC$^+$CD11c$^+$MHC II$^+$ cells) to DLNs (Fig. 4B, 4C). Further phenotypic analysis indicated that recruited DC populations bearing the cell tracker were mainly CD8α$^+$CD11b$^-$ CD103$^+$CD207$^+$ DCs and CD8α$^-$CD11b$^+$CD103$^-$CD207$^-$ DCs (Fig. 4B, 4D, $p < 0.001$ versus dextran-FITC alone). Similarly, coinjection of U-Omp19 increased the recruitment of dextran-FITC$^+$CD11b$^+$CD11c$^-$ cells to DLNs. Among these cells, the increment was mainly due to dextran-FITC$^+$CD11b$^+$CD11c$^-$ Ly6C^{high} inflammatory monocytes and to dextran-FITC$^+$CD11b$^+$ CD11c$^-$Ly6G$^+$ neutrophils (Fig. 4C, 4D, $p < 0.05$ or $p < 0.001$ versus dextran-FITC alone).

DC recruitment was also assessed by adoptive transfer of GFP BMDCs. GFP DCs were stimulated for 18 h with medium alone, U-Omp19, or LPS and then s.c. injected into recipient wild-type mice. After 12 h, DLN cells were analyzed for the presence of GFP donor DCs by flow cytometry. U-Omp19 increased the migration of GFP DCs to DLNs in comparison with nonstimulated GFP DCs (Fig. 4E, $p < 0.05$ versus medium alone).

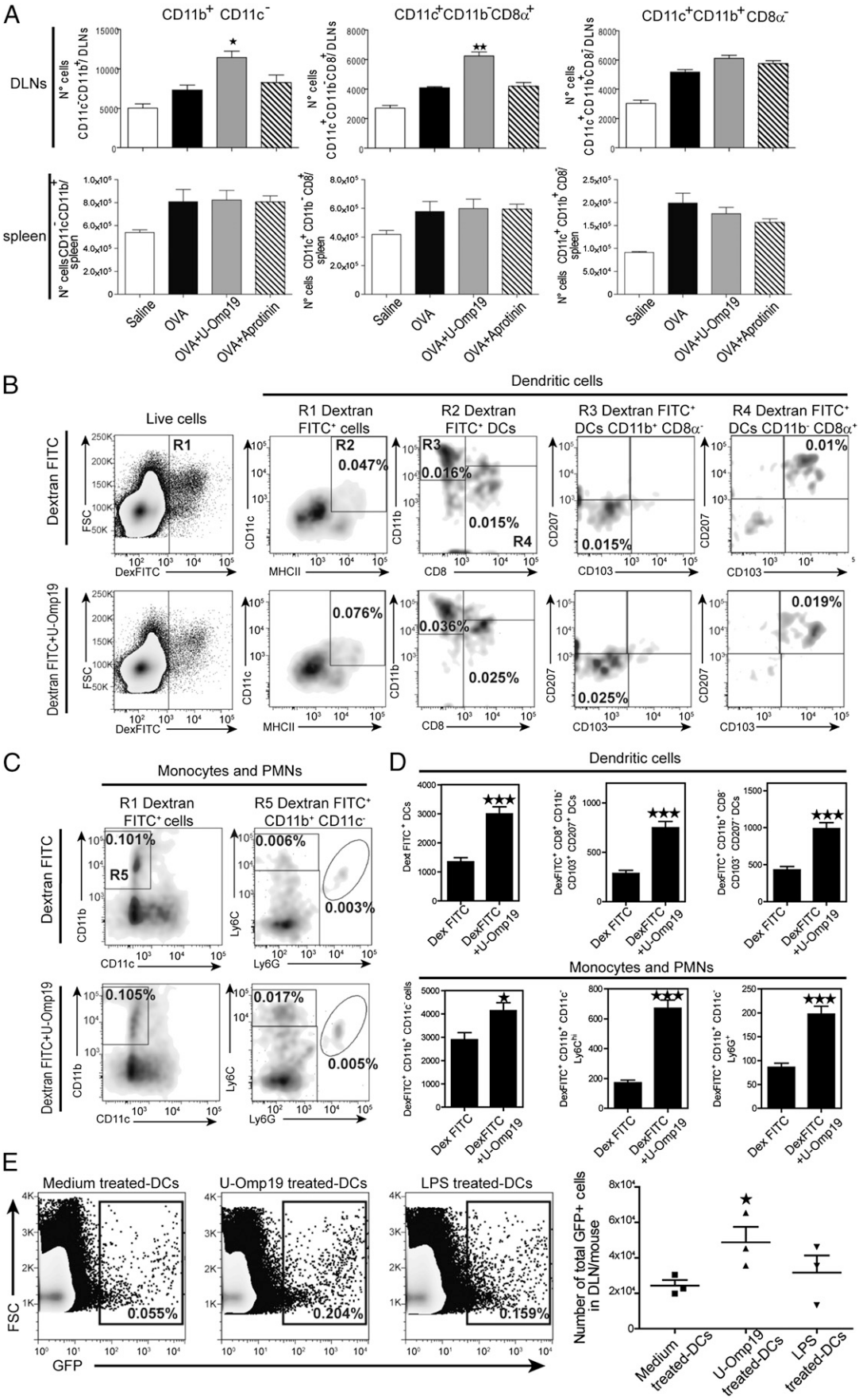

FIGURE 4. Subcutaneous administration of U-Omp19 induces APC recruitment to DLNs in vivo. (**A**) Flow cytometric analysis of $CD11b^+CD11c^-$, $CD11c^+CD11b^-CD8\alpha^+$, and $CD11c^+CD11b^+CD8\alpha^-$ cells from DLNs at 18 h after s.c. delivery of OVA, OVA plus U-Omp19, OVA plus aprotinin, or saline to mice ($n = 3$/group). Results are presented as the mean total number of cells from each specified population obtained for (*Figure legend continues*)

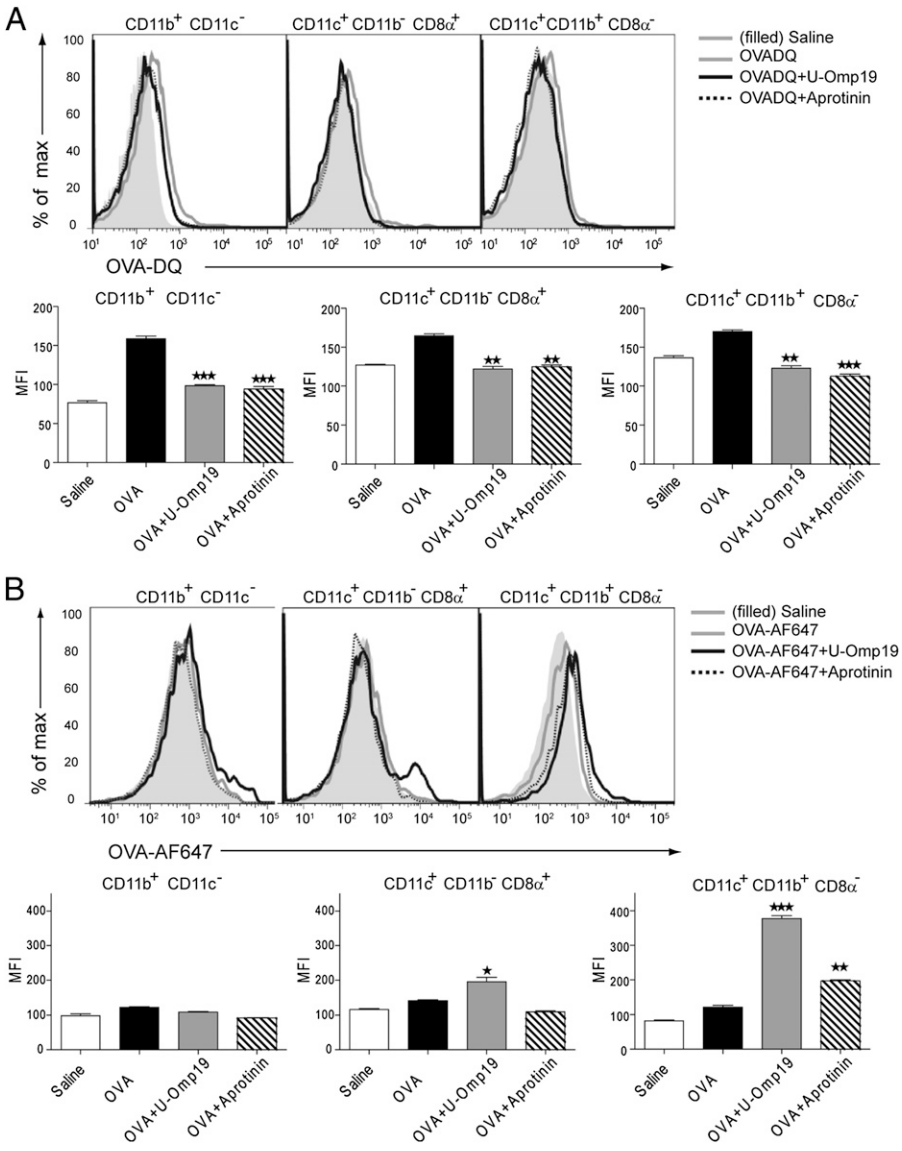

FIGURE 5. U-Omp19 reduces Ag degradation inside APCs after its coadministration in vivo. Flow cytometric evaluation of Ag degradation and amount status in recruited APCs after s.c. delivery of OVADQ (**A**) and OVA–Alexa Fluor 647 (**B**) alone or plus U-Omp19 or aprotinin. Results are presented as representative histograms and as mean fluorescence intensity (MFI) ± SEM obtained for each group (n = 3/group) and are representative of three different experiments ($^{\star}p < 0.05$, $^{\star\star}p < 0.01$, $^{\star\star\star}p < 0.001$ versus OVA group).

To evaluate Ag proteolysis and amount inside APCs from DLNs in vivo, BALB/c mice were s.c. inoculated with OVADQ and OVA–Alexa Fluor 647 simultaneously plus buffer, U-Omp19, or aprotinin as control. Consistent with our in vitro results, Ag inside monocytes ($CD11b^+MHC\ II^+CD11c^-CD8\alpha^-$, $p < 0.001$ versus OVA) and conventional DCs ($CD11c^+CD11b^-CD8\alpha^+$ and $CD11c^+CD11b^+CD8\alpha^-$, $p < 0.01$ versus OVA) was less digested when it was codelivered with U-Omp19 (Fig. 5A).Therefore, U-Omp19 reduces Ag digestion within APCs after its coadministration in vivo. Consequently, a greater amount of Ag in DLN cells from mice immunized s.c with U-Omp19 plus OVA was found in both DCs subpopulations ($CD11c^+CD11b^-CD8\alpha^+$ and $CD11c^+CD11b^-CD8\alpha^-$, $p < 0.05$ and $p < 0.001$ versus OVA) (Fig. 5B).

These findings indicate that U-Omp19 recruits APCs to inductive sites, reduces Ag digestion inside APCs, and promotes Ag retention in lymph nodes for extended periods of time.

U-Omp19 retains the Ag in Lamp-2$^+$ endosomal compartments after its internalization by DCs

To address the intracellular Ag fate after its coadministration with U-Omp19, the Ag localization in subcellular compartments was analyzed by confocal microscopy. BMDCs were pulsed with OVA–Alexa Fluor 647 (blue) alone or with U-Omp19 (green) and labeled with the endolysosomal associated marker Lamp-2 (red) or with the early endosomal marker Rab-5 (red). Thirty minutes after OVA codelivery with U-Omp19, OVA was excluded from Lamp-2^+ compartments whereas after 1 h OVA was mainly concentrated

each mouse ± SEM and are representative of two different experiments ($^{\star}p < 0.05$, $^{\star\star}p < 0.01$ versus number of cells in OVA group). Flow cytometric analyses of DC (**B**), monocyte, and polymorphonuclear neutrophil (PMN) (**C**) subsets recruited 18 h after s.c. administration of dextran-FITC or dextran-FITC plus U-Omp19. Live cells were gated using Zombie Aqua viability dye. Flow cytometry plots indicate percentages of live cells. Results are presented as the mean total numbers of cells from each specified population obtained for each mouse ± SEM (**D**) and are representative of two different experiments ($^{\star}p < 0.05$, $^{\star\star\star}p < 0.001$ versus dextran-FITC). (**E**) Migration of GFP BMDCs to DLNs. BDMCs were incubated for 18 h with medium, U-Omp19, or LPS and then s.c. injected to wild-type mice (n = 3/group), and 12 h later DLNs were obtained and the presence of GFP^+ DCs was analyzed by flow cytometry. Dot plots are representative of each group of mice and indicate percentages of live cells. The mean total number of GFP^+ cells in DLNs from each mouse ± SEM is shown ($^{\star}p < 0.05$ versus medium-treated DCs).

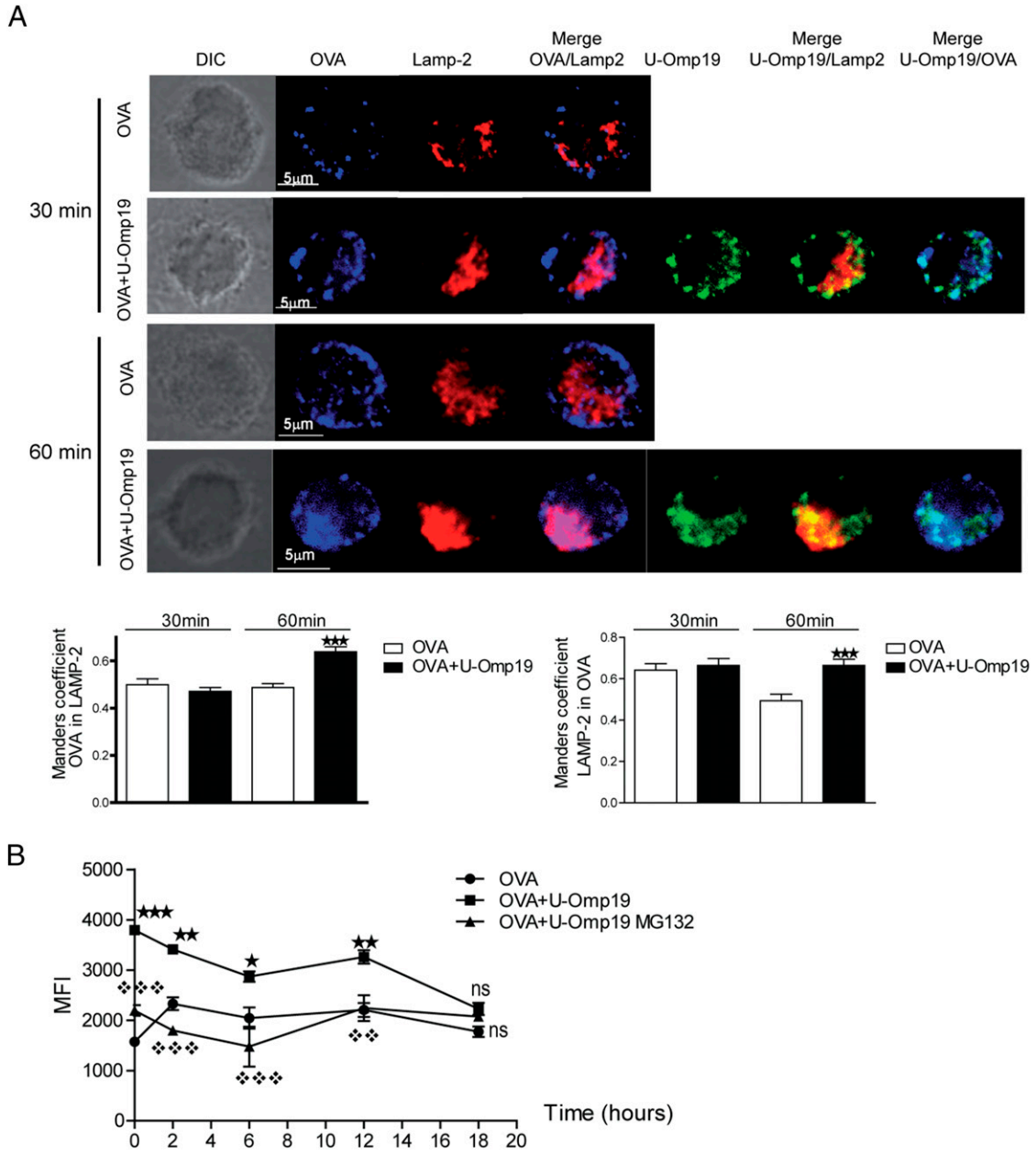

FIGURE 6. U-Omp19 retains the Ag in Lamp-2$^+$ endosomal compartments after its internalization, increasing Ag cross-presentation by DCs. (**A**) Confocal scanning microscopy analysis of BMDCs treated with OVA–Alexa Fluor 647 (blue) alone or plus U-Omp19. After 30 and 60 min of incubation, cells were fixed, permeabilized, and stained with polyclonal Ab rabbit anti-Omp19 or mAb mouse anti–Lamp-2. Anti-rabbit IgG coupled to Alexa Fluor 488 (green) and anti-mouse IgG coupled to Alexa Fluor 546 (red) were used as secondary Abs. Images are representative of most cells examined by confocal microscopy. The overlap between Lamp-2/OVA, Lamp-2/U-Omp19, and U-Omp19/OVA is shown. Quantification of colocalization OVA/Lamp-2 (M1) and Lamp-2/OVA (M2) was analyzed by Manders' overlap coefficient calculation. Data are means of Manders' coefficients ± SEM from 200 ROI (lysosomes) present in five images of each condition. Results are representative of two independent experiments ($^{\star\star\star}p < 0.001$ versus OVA). (**B**) BMDCs were pulsed with OVA alone or plus U-Omp19 during 1 h. MG132 was used as a proteasome inhibitor. Then, the Ag was removed and chased at different times (0, 2, 6, 12, and 18 h). Evaluation of $OVA_{257–264}$/H-2K^b complex expression was performed using the mAb 25D1.16. Results are representative of three different experiments. Data are represented as mean fluorescence intensity (MFI) ± SEM ($^{\star}p < 0.05$, $^{\star\star}p < 0.01$, $^{\star\star\star}p < 0.001$ versus OVA group; $^{\clubsuit\clubsuit}p < 0.01$, $^{\clubsuit\clubsuit\clubsuit}p < 0.001$ versus OVA plus U-Omp19 group).

in Lamp-2$^+$ compartments (significant increase in Manders' colocalization coefficient M1 and M2 between OVA and Lamp-2 signal, $p < 0.001$ versus OVA alone) (Fig. 6A). In contrast, incubation with OVA alone showed a small protein amount, mostly in the periphery, excluded from Lamp-2$^+$ compartments, suggesting that OVA was digested when delivered alone. Additionally, U-Omp19 is present in Lamp-2$^+$ compartments, suggesting that the presence of the protease inhibitor inside the lysosome is required to delay Ag degradation in this compartment (Fig. 6A).

It has been proposed that soluble OVA is delivered to Rab-5 early endosomal compartments after its uptake by mannose receptor. In this compartment, OVA cross-presentation is mediated by a protease-independent mechanism alternative to the endogenous MHC I–restricted pathway (15, 32). Therefore, we further evaluated its presence in these compartments. Coincubation of

OVA plus U-Omp19 did not modify the presence of OVA in Rab-5$^+$ compartments (Supplemental Fig. 3A).

Collectively, these data indicate that U-Omp19 does not alter the intracellular traffic of OVA through vesicular compartments but promotes the accumulation of OVA in internal Lamp-2$^+$ endosomal compartments, likely due to reduced or delayed intracellular degradation by endosomal cysteine proteases.

U-Omp19 promotes a sustained expression of $OVA_{257–264}$/H-2K^b complexes in the cell surface of DCs

To evaluate whether the intracellular inhibition of Ag degradation by U-Omp19 resulted in an enhanced Ag cross-presentation, BMDCs were pulsed with OVA alone or with U-Omp19, and then the cells were washed to remove the remaining noninternalized Ag. The generation of $OVA_{257–264}$/H-2K^b complexes was evaluated using an mAb that recognizes $SIINFEKL_{257–264}$ peptide from OVA bound to H-2K^b molecules at different times points (33). DCs pulsed with OVA plus U-Omp19 showed an increment in cell surface $OVA_{257–264}$/H-2K^b complexes ($p < 0.01$ versus OVA) detectable for up to 12 h (Fig. 6B, Supplemental Fig. 3B). Treatment with proteasome inhibitor MG132 prevented the formation of MHC I/SIINFEKL complexes, indicating that U-Omp19 enhances cross-presentation of OVA by a proteasome-dependent mechanism ($p < 0.001$ versus OVA plus U-Omp19) (Fig. 6B). Limited Ag proteolysis within lysosomal compartments would result in an extended source of intact peptides for export into the cytosol, leading to the long-lasting peptide cross-presentation observed when U-Omp19 was codelivered.

U-Omp19 facilitates OVA cross-presentation by DCs

Given that a limited Ag proteolysis inside DCs due to U-Omp19 codelivery delays Ag processing promoting Ag cross-presentation, the ability of U-Omp19 to enhance activation of CD8$^+$ T cells by DCs was examined. To assess this, BMDCs from C57BL/6 mice were treated with OVA alone or plus U-Omp19 and then cocultivated with OT-I CD8$^+$ T cells. OT-I transgenic T cells that were in contact with DCs incubated with OVA plus U-Omp19 showed a higher activation profile (downregulated CD62L expression) and IFN-γ production compared with T cells cocultivated with DCs pulsed with OVA alone (Fig. 7A, 7B, $p < 0.05$ and $p < 0.001$ versus OVA alone). Moreover, these cells presented greater CD107a expression on the membrane accordingly with a CTL phenotype (Fig. 7C, $p < 0.01$ versus OVA alone). U-Omp19 digested with PK was used as a negative control. Treatment with U-Omp19PK did not induce activation, IFN-γ production, or CD107a expression.

To extend our results using a different Ag, we used a soluble chimeric GFP containing the SIINFEKL MHC I–restricted peptide epitope, which is recognized by CD8$^+$ OT-I cells. This chimeric protein is not internalized by C-type lectin-like receptors such as OVA (28). After coincubation of GFP OT-I plus U-Omp19, DCs were able to increase Ag cross-presentation to CD8$^+$ T cells, as revealed by a greater percentage of IFN-γ–producing OT-I cells compared with incubation with GFP OT-I alone (Fig. 7D, $p < 0.01$ versus OVA alone). Leupeptin or aprotinin coincubation were not as good as U-Omp19 to enhance CD8$^+$ T cellular immune responses (Fig. 7D).

Next, cross-presentation capacity by DCs was evaluated in the presence or absence of LPS stimulation plus medium, OVA, OVA plus U-Omp19, OVA plus leupeptin, or OVA plus cystatin C. As stated before, U-Omp19 plus OVA in the absence of the TLR ligand LPS induced a significant increase in CD8$^+$ T cell cross-presentation by DCs cells in comparison with OVA alone ($p < 0.05$ versus OVA). In the presence of LPS, U-Omp19 induced a similar increase in cross-presentation than when without LPS (Fig. 7E). This result indicates that U-Omp19 can enhance Ag cross-presentation without the requirement of an external DC-activating molecule. In contrast, leupeptin or cystatin C only induced cross-presentation when DCs were incubated with LPS (Fig. 7E). Of note, there was a slight but statistically significant reduction of cross-presentation in leupeptin plus OVA or cystatin C plus OVA plus LPS– versus OVA plus LPS–stimulated cells ($p < 0.001$ versus OVA plus LPS), suggesting that these protease inhibitors would have downmodulating immune activity.

To evaluate the contribution of the protease inhibitor activity of U-Omp19 in the outcome of CD8$^+$ T cell immune responses, DCs in absence or presence of LPS were pulsed with different OVA doses and the capacity of U-Omp19 to enhance cross-presentation was analyzed. In the absence of LPS, OVA alone at the different doses assessed did not induce Ag cross-presentation. In the presence of LPS there was a significant increase in cross-presentation induced by OVA alone at the highest dose (50 μg/ml; $p < 0.001$ versus OVA [50 μg/ml] without LPS), but there was a significant reduction at lower doses of Ag (25 and 5 μg/ml; $p < 0.001$ versus OVA [50 μg/ml] plus LPS), showing the contribution of LPS stimulation and the Ag dose in the outcome of the elicited immune response (Fig. 7F). Results also indicate that U-Omp19 increased OVA cross-presentation in a dose-dependent manner in absence of LPS ($p < 0.001$ versus OVA without LPS). Note that in presence of LPS and at lower Ag doses (25 and 5 μg/ml) there was a significant increase in Ag cross-presentation in OVA plus LPS plus U-Omp19 in comparison with OVA plus LPS (Fig. 7F, $p < 0.001$ versus OVA 25 μg/ml or OVA 5 μg/ml, both plus LPS). This result suggests an additive effect of U-Omp19 due to its capacity to limit Ag digestion and consequently increase Ag half-life (Ag dose) inside DCs.

In conclusion, U-Omp19 has adjuvant properties when codelivered with an Ag: it facilitates Ag cross-presentation and induces IFN-γ–producing CD8$^+$ T cells.

U-Omp19 enhances CD8$^+$ T cell proliferation in vivo

Adoptive transfer assays using TCR transgenic mice OT-I were performed to determine in vivo the primary Ag-specific clonal expansion of transgenic CFSE$^+$-labeled T cells following s.c. immunization. After 3 d, mice s.c. immunized with OVA coadministered with U-Omp19 showed a greater CD8$^+$ T cell proliferation in spleen and DLNs than mice immunized with OVA alone (Fig. 8A, $p < 0.05$ versus OVA alone). A high OT-I proliferation was also induced after LPS administration. Consistently with in vitro results, OVA s.c. coadministered with leupeptin or cystatin C failed to increase OT-I proliferation at spleens or DLNs (Fig. 8B). These results suggest that U-Omp19 coadministered as adjuvant enhances cross-presentation of soluble OVA by DCs in vivo.

U-Omp19 s.c. coadministered with OVA induces CD8$^+$ T cell immune responses in vivo and extends the survival of mice after tumor challenge

To evaluate the CD8$^+$ T cell immune response induced upon coadministration of U-Omp19 and OVA in vivo, mice were s.c. immunized on days 0, 7, and 14. OVA-specific IFN-γ–producing CD8$^+$ T cells were determined 3 wk after the last immunization. Immunization with OVA plus U-Omp19 induced a higher percentage of IFN-γ–producing CD8$^+$ T cells (1.4%) compared with immunization with OVA alone (0.6%) (Fig. 9A). CFA, a known potent but unsafe adjuvant induced a smaller CD8$^+$ T cell response against the coadministered Ag (0.9%) (Fig. 9A).

Then, the in vivo antitumoral capacity of elicited CD8$^+$ T cells after U-Omp19 coimmunization was assayed. To conduct this, C57BL/6 mice were inoculated s.c. with OVA, OVA plus U-Omp19,

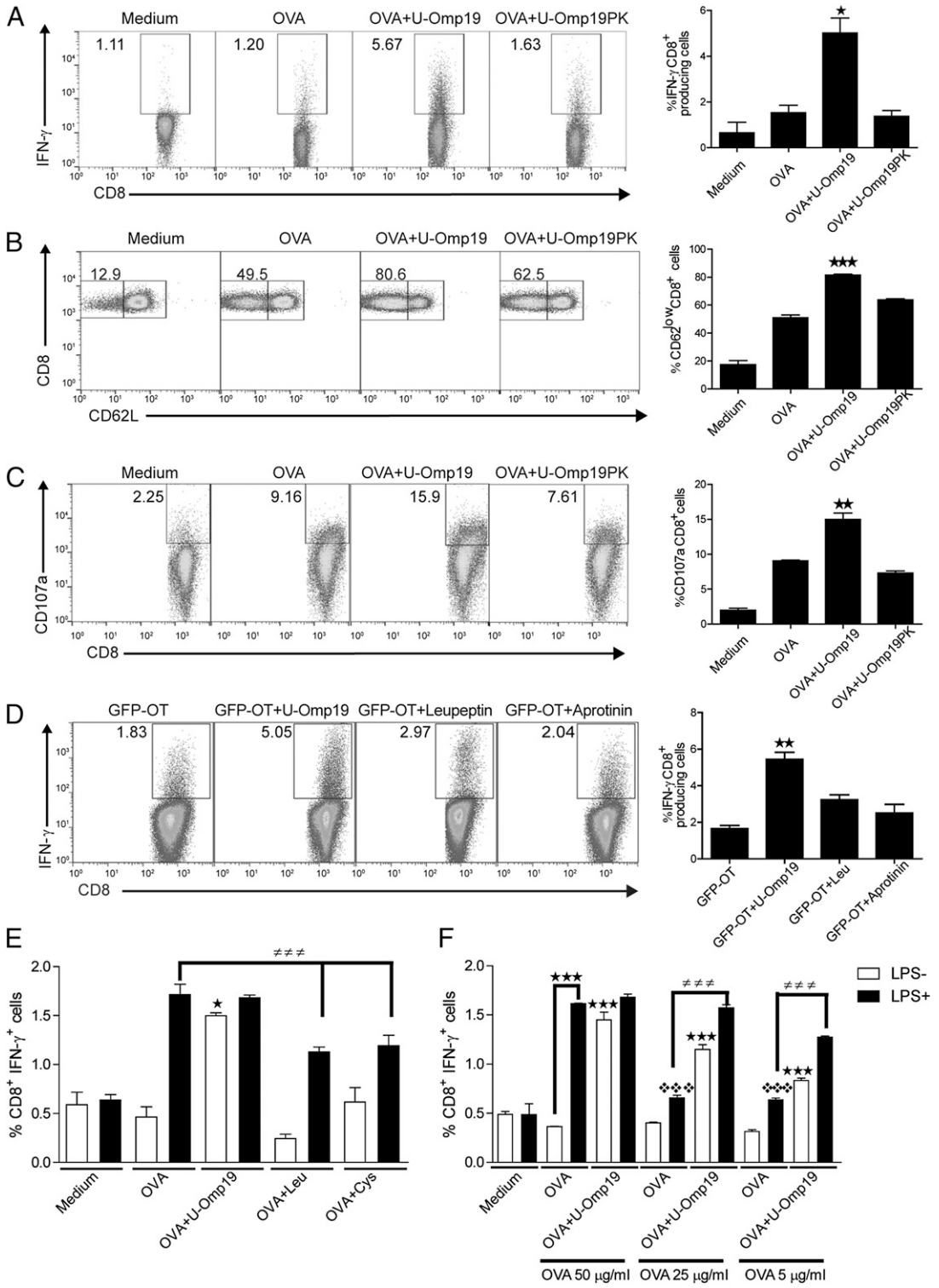

FIGURE 7. U-Omp19 increases Ag cross-presentation by DCs in vitro. BMDCs ($CD11c^+MHC\ II^{low}$) were stimulated with complete medium, OVA, OVA plus U-Omp19, or OVA plus U-Omp19PK for 18 h and then washed and cocultured in vitro with OT-I cells. Anti-CD107 was added during the last 6 h, and brefeldin A and monensin were added during the last 5 h of culture. Afterward, cells were harvested and stained with specific Abs anti-CD8 and anti-CD62L, fixed, permeabilized, and stained intracellularly with anti–IFN-γ Ab. Results are presented as percentage of IFN-γ–producing $CD8^+$ T lymphocytes (**A**), percentage of $CD62L^{low}CD8^+$ T cells (**B**), and percentage of $CD107a^+CD8^+$ T cells (**C**) ± SEM. Results are representative of three independent experiments ($^\star p < 0.05$, $^{\star\star} p < 0.01$ versus OVA group). (**D**) BMDCs were stimulated with GFP OT-I chimera, GFP OT-I plus U-Omp19, GFP OT-I plus leupeptin, or GFP OT-I plus aprotinin for 18 h, and then washed and cocultured in vitro with OT-I cells. For the last 5 h, cells were treated with brefeldin A. Afterward, cells were harvested and stained with specific Ab anti-CD8, fixed, permeabilized, and stained intracellularly with anti–IFN-γ Ab. Results are presented as percentage of IFN-γ–producing $CD8^+$ T cells ± SEM ($^{\star\star} p < 0.01$ versus GFP OT-I group). Data are representative of three different experiments. (**E**) Cross-presentation capacity of BMDCs pulsed with complete medium, OVA (50 μg/ml), OVA plus U-Omp19, OVA plus leupeptin, or OVA plus cystatin C in the presence or absence of LPS. (**F**) Cross-presentation capacity of BMDCs pulsed with complete medium, OVA (different doses of 50, 25 or 5 μg/ml), or OVA plus U-Omp19 in the presence or absence of LPS. In (E) and (F), cells were then washed and cocultured in vitro with OT-I cells. Next, cells were stained with anti-CD8 Ab and intracellularly with anti-IFN-γ (*Figure legend continues*)

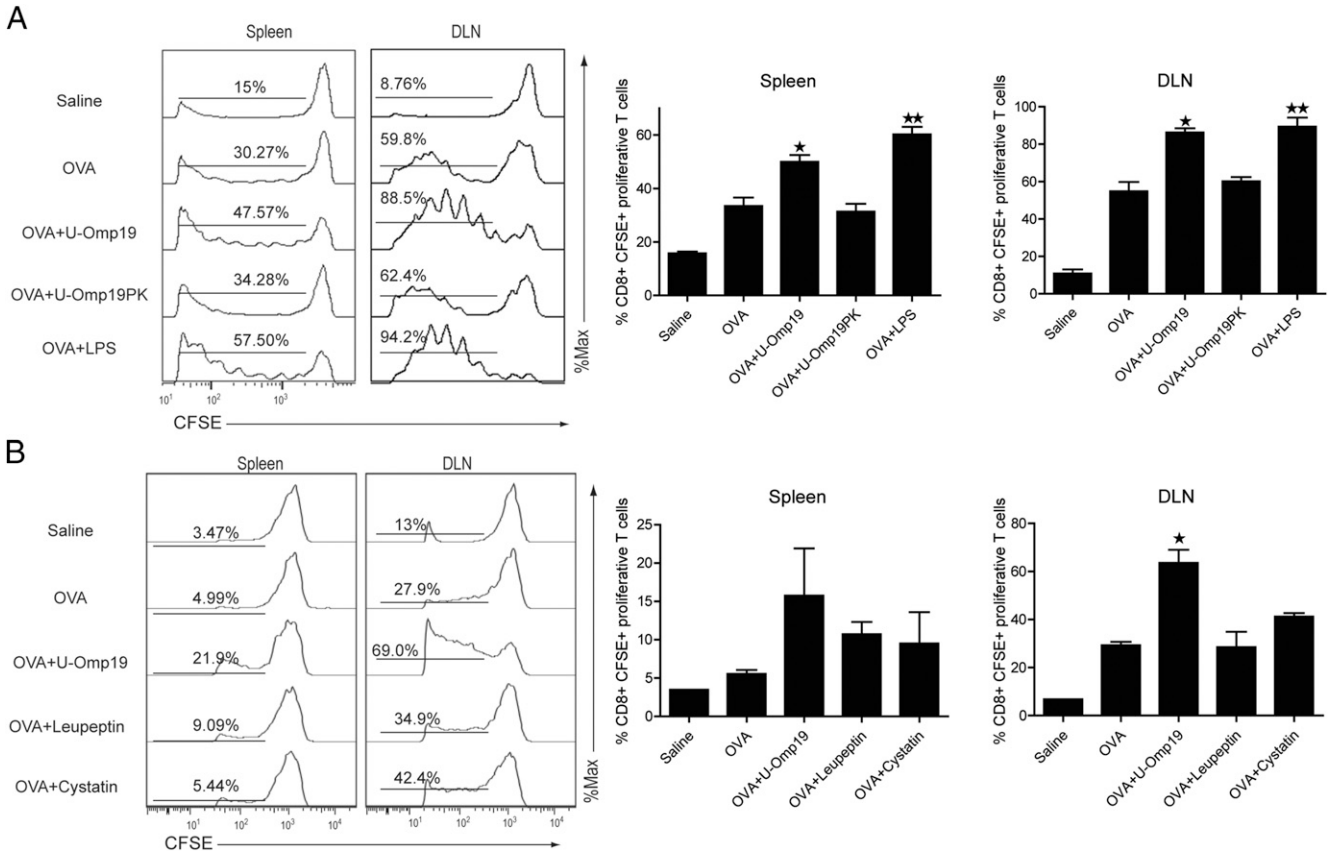

FIGURE 8. U-Omp19 induces T CD8$^+$ cell proliferation in vivo. (**A**) Proliferation in vivo of OT-I CD8$^+$ CFSE labeled T cells after s.c. administration (n = 3/group) of saline, OVA, OVA plus U-Omp19, OVA plus U-Omp19PK, or OVA plus LPS. (**B**) Proliferation of OT-I CD8$^+$ CFSE-labeled T cells after s.c. administration (n = 3/group) of saline, OVA, OVA plus U-Omp19, OVA plus leupeptin, or OVA plus cystatin C. In (A) and (B), 5 d later spleen and DLNs were obtained and cell suspensions were analyzed by flow cytometry. Results are shown as representative histograms, and data are represented as percentage of OT-I CD8$^+$CFSE$^+$ proliferative T cells ± SEM. Data are representative of two different experiments. $^{\star}p < 0.05$, $^{\star\star}p < 0.01$ versus OVA group.

or OVA plus CFA. Three weeks after the last immunization, tumor challenge was s.c performed using OVA-transfected B16 melanoma tumor cells. Animals immunized with OVA plus U-Omp19 or CFA significantly increased survival rates after tumor challenge in comparison with the OVA-immunized group (Fig. 9B). About 85% of mice immunized with OVA plus U-Omp19 survived following day 30 after challenge; in contrast, immunization with OVA alone showed a 40% survival at this time point. At day 35, ~65% of mice remained alive in the group OVA plus U-Omp19, whereas no mice survived in the OVA group (Fig. 9B, $p < 0.05$ versus OVA). Thus, the induction of CD8$^+$ T cells against OVA allowed an antitumor response after s.c. codelivery with U-Omp19.

Collectively, these results indicate that U-Omp19 induces CD8$^+$ T cell immune responses in vivo and thus could be a suitable component in future vaccine formulations against tumors.

Discussion

It is known that without Ag processing into MHC I and II, induction of adaptive immune responses cannot proceed. However, Ags more resistant to lysosomal proteolysis induce more robust immune responses (11, 34). In this study, we demonstrated that U-Omp19, a *Brucella* spp. protein, has cysteine protease inhibitor activity.

We examined whether U-Omp19 protease inhibitor activity can affect Ag degradation inside APCs. U-Omp19 partially inhibited (30–35%) the activity of cysteine proteases (cathepsin B, L, and C and papain) in vitro and the proteolytic capacity in live BMDCs and BMDMs. It was demonstrated by different approaches (fluorimetry, flow cytometry, and confocal microscopy) that U-Omp19 partially inhibits cathepsin L activity inside live DC lysosomes. Moreover, U-Omp19 inhibits cathepsin L activity inside live mature DCs (LPS treated), indicating that observed inhibition by U-Omp19 is not an indirect consequence of changes undertaken by DCs during maturation (29).

Additionally, it was established by kinetic assays that U-Omp19 has a competitive mechanism of inhibition of human cathepsin L with an inhibition constant in the micromolar range (K_i = 2 μM). Most protease inhibitors bind in and block access to the active site of their target protease, but they do not bind in a strictly substrate-like manner. Instead, they interact with the protease subsites and catalytic residues in a non–catalytically competent manner. The cystatins, a superfamily of proteins that inhibit papain-like cysteine proteases, are a classic example of these inhibitors (35). When we compare the protease inhibitor activity of U-Omp19 with other endogenous (host cystatins) or exogenous (leupeptin, E-64) cysteine protease inhibitors that have dissociation constants in the picomolar and nanomolar range, respectively, U-Omp19 is

Ab as described in (A). Results are presented as percentage of IFN-γ–producing CD8$^+$ T cells ± SEM. ($^{\star}p < 0.05$, $^{\star\star\star}p < 0.001$ versus the same concentration of OVA without LPS; $^{\neq\neq\neq}p < 0.001$ versus the same concentration of OVA plus LPS; $^{\diamond\diamond\diamond}p < 0.001$ versus OVA 50 plus LPS).

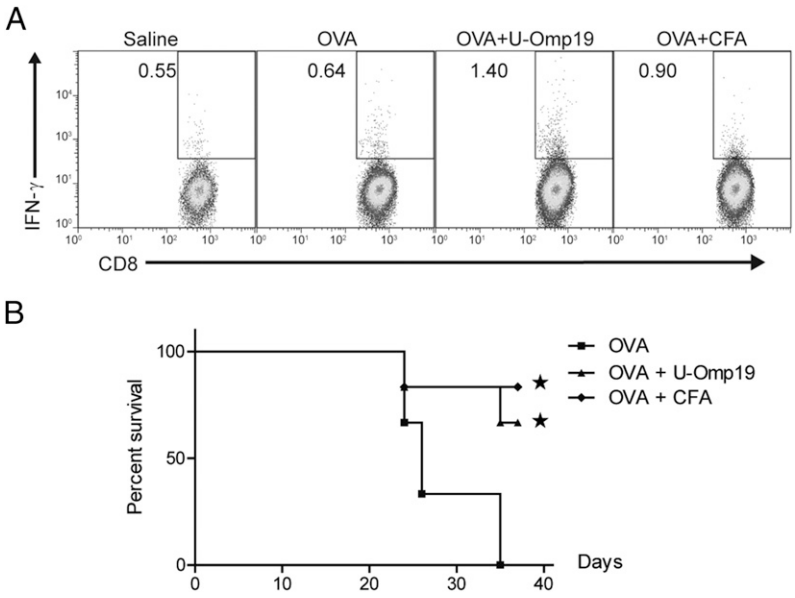

FIGURE 9. U-Omp19 coadministration induces $CD8^+$ T cell responses in vivo and protects against tumor challenge. Mice (n = 3/group) were s.c. immunized with saline, OVA, OVA plus U-Omp19, or OVA plus CFA. (**A**) Three weeks later, splenocytes from immunized mice were cultured in presence of complete medium or Ag stimuli for 18 h. Next, brefeldin A was added for 5 h more to the samples. After that, cells were harvested and stained with anti-CD8, fixed, permeabilized, and stained with anti–IFN-γ Ab and analyzed by flow cytometry. (**B**) C57BL/6 mice (n = 6/group) were s.c. immunized with OVA, OVA plus U-Omp19, or OVA plus CFA. Three weeks later, mice were challenged with B16 expressing OVA melanoma cells. Representative of two different experiments. Results are shown as percentage of survival of mice in a Kaplan–Meier curve ($^\star p < 0.05$ versus OVA group).

less potent as a cysteine protease inhibitor (Supplemental Fig. 4A). A potent Ag degradation inhibition may block Ag presentation, avoiding the induction of an immune response, and in this way the moderate inhibitor activity of U-Omp19 is an attractive feature, as it is proposed as a component for a subunit vaccine formulation.

Consistent with our findings, it was reported that DCs, which are the most efficient APCs, are less efficient in breaking down endocytosed Ags compared with macrophages. Whereas the macrophages contain high levels of lysosomal proteases and rapidly degrade internalized Ags, DCs express lower levels of lysosomal proteases and degrade internalized Ags slowly. The limited lysosomal proteolysis in DCs favors Ag presentation (10).

A partial reduction of Ag degradation is advantageous not only in terms of preservation of intact Ag epitopes to be presented but also in terms of T cell activation. Recently it has been reported that only T cells that interact with DCs pulsed with a high dose of Ag gave rise to sustained immunological memory (5). We confirmed that the higher Ag amount observed when U-Omp19 is codelivered to APCs is not due to an increase in Ag uptake (pinocytosis or phagocytosis); instead, it is a result of the limited Ag digestion triggering Ag accumulation inside cells. Of note, we confirmed that the observed increase in the amount of protein Ag inside APCs when U-Omp19 is codelivered is not a consequence of DC maturation because similar uptake has been observed in LPS-treated and nontreated DCs. We have also demonstrated that there are no differences in the intracellular pH that might further diminish lysosomal function as occurs in $CD8\alpha^+$ DCs (36–38) or different levels of protease content that can explain the reduction in Ag degradation promoted by U-Omp19.

Furthermore, immunofluorescence confocal microscopy studies codelivering U-Omp19 and OVA to BMDCs show that both proteins are within lysosomes, and the amount of Ag in this compartment is higher than when it is delivered alone. This suggests that the presence of the protease inhibitor inside the lysosome is required to delay Ag degradation. The fact that inhibiting proteolysis enhances the ability of late endosomes and lysosomes to allow cross-presentation of accumulated Ags was studied by measuring the formation of OVA peptide/MHC I at the surface of DCs. After incubation of soluble OVA with U-Omp19, there was a significant increase in OVA peptide/MHC I complexes. U-Omp19 may promote less degradation of peptide Ags, which increases their ability to persist long enough to escape into the cytosol and be presented in MHC I molecules. It has been reported that another adjuvant compound (ISCOMATRIX) is able to induce an efficient cross-presentation of Ag by promoting a rapid Ag translocation to the cytosol in DCs (39). The oil-in-water emulsion adjuvant MF59 can persist in DLNs, promoting accumulation of the unprocessed Ag. Ag retention within lymph nodes is critical for the development of adaptive immune responses, because it facilitates the encounter of the Ag with cognate lymphocytes (40).

In mice, there is evidence indicating that the $CD8\alpha^+$ DC subset plays a key role in Ag cross-presentation in vivo (41, 42). In agreement with these findings, U-Omp19 induces recruitment of $CD11c^+CD8\alpha^+$ cells at inductive sites after s.c. delivery with OVA. U-Omp19 codelivery limits Ag degradation and consequently increases the amount of Ag within this DC population compared with the delivery of Ag alone. Accordingly, in vitro cross-presentation and in vivo T cell proliferation assays showed a greater capacity of U-Omp19 to induce the activation, proliferation, and production of IFN-γ by $CD8^+$ T cells. In contrast, leupeptin, cystatin C, or aprotinin could not induce IFN-γ–producing $CD8^+$ T cells.

Thus, we demonstrated that potent cysteine protease inhibitors such as leupeptin or human cystatin C are able to reduce degradation of Ags but are not inductors of $CD8^+$ T cell immune responses. Furthermore, it has been suggested that cystatin-type molecules secreted from parasites downmodulate the host immune response (43–45). Thus, every protease inhibitor, depending on its particular structure, mechanism of action, and potency, may have different immunomodulatory properties that should be studied in detail.

It has been previously demonstrated that U-Omp19 induces the maturation of DCs in vivo (20). In this study, we demonstrated that U-Omp19 induces the upregulation of costimulatory molecules (CD86, CD40) by BMDCs in vitro whereas a known protease inhibitor such as leupeptin does not (Supplemental Fig. 4B). In contrast to most studied protease inhibitors that were found to be immunoregulatory and anti-inflammatory (43–45), U-Omp19 has inflammatory properties, as it induces the activation of DCs and recruitment of APCs at inductive sites. Analysis of NF-κB activation in HEK293 reporter cells expressing a given TLR/Nod-like receptor (InvivoGen pattern recognition receptor ligand screening service) demonstrated that U-Omp19 does not signal through

mouse TLR2, 3, 4, 7, 8, 9, and 13 or mouse Nod-like receptors (NOD1 and NOD2) (data not shown). Importantly, note that at present there are adjuvants used in human vaccine formulations, such as MF59, known to have important inflammatory properties and that are safe, but to which their innate receptor has not been found until present. MF59 significantly increases the number of Ag-loaded APCs in DLNs compared with nonadjuvanted vaccine (46).

Despite that limiting proteolysis can favor Ag presentation by APCs, the activation of T cells by DCs requires at least two signals to become fully activated. The first occurs after engagement of the TCR by the MHC, and the second comprises the recognition of costimulatory molecules in the DC surface. Sensing signal 1, in the absence of signal 2, leads to T cell anergy. Alternatively, an activated-mature DC bearing a subthreshold Ag dose (low Ag dose or low persistence) could not efficiently activate T cells (5, 47). Hence, we proposed that codelivery of U-Omp19 increases $CD8^+$ T cell responses by 1) partially limiting lysosome activity that permits the Ag to be exposed for longer periods of time, promoting a sustained Ag cross-presentation, and 2) having immunostimulatory properties on APCs. Having these capacities makes U-Omp19 a singular protease inhibitor.

Additionally, coadministration of U-Omp19 increases the survival of mice in a melanoma model expressing OVA, suggesting that it induces functional $CD8^+$ T cell antitumoral immune responses in vivo.

Protease inhibitors have emerged as a powerful drug class. At present, many protease inhibitors are used for treatment of different diseases. They include ACE inhibitors for treating high blood pressure, HIV-1 protease inhibitors for treating HIV/AIDS, thrombin inhibitors for treating stroke, an elastase inhibitor for treating systemic inflammatory response syndrome, and proteasomal inhibitors such as bortezomib (Velcade) used to treat multiple myeloma (48, 49). Although lysosomal proteases have been proposed as therapeutic targets, at present there are no studies of lysosome protease inhibitors used as adjuvants in vaccine formulations to increase immune responses. Therefore, our results will lead to a new concept in immune vaccine delivery and immunointervention.

Acknowledgments

We thank Dr. Sergio Trombetta (New York University) for providing the GFP OT-I chimera and for scientific advice and help on protocols to obtain APC microsomes and internalization experiments.

Disclosures

L.M.C., A.E.I., G.H.G., K.A.P., and J.C. are inventors on a patent related to U-Omp19. This patent, presented by the authors' National Research Council, "Adjuvant for vaccines, vaccines that comprise it and uses," presentation P 20090104015, was filed on October 19, 2009 in the National Institute of Intellectual Property, Argentina. This patent was also filed on October 18, 2010 in the European Patent Office, Spain PCT/ES2010/070667. The filing of the patent did not have any role in experimental design, data collection and analysis, decision to publish, or preparation of this manuscript. The authors have no financial conflicts of interest.

References

1. Awate, S., L. A. Babiuk, and G. Mutwiri. 2013. Mechanisms of action of adjuvants. *Front. Immunol.* 4: 114.
2. Obst, R., H. M. van Santen, D. Mathis, and C. Benoist. 2005. Antigen persistence is required throughout the expansion phase of a $CD4^+$ T cell response. *J. Exp. Med.* 201: 1555–1565.
3. Iezzi, G., K. Karjalainen, and A. Lanzavecchia. 1998. The duration of antigenic stimulation determines the fate of naive and effector T cells. *Immunity* 8: 89–95.
4. Obst, R., H. M. van Santen, R. Melamed, A. O. Kamphorst, C. Benoist, and D. Mathis. 2007. Sustained antigen presentation can promote an immunogenic T cell response, like dendritic cell activation. *Proc. Natl. Acad. Sci. USA* 104: 15460–15465.
5. Henrickson, S. E., M. Perro, S. M. Loughhead, B. Senman, S. Stutte, M. Quigley, G. Alexe, M. Iannacone, M. P. Flynn, S. Omid, et al. 2013. Antigen availability determines $CD8^+$ T cell-dendritic cell interaction kinetics and memory fate decisions. *Immunity* 39: 496–507.
6. Conus, S., and H.-U. Simon. 2010. Cathepsins and their involvement in immune responses. *Swiss Med. Wkly.* 140: w13042.
7. Turk, V., V. Stoka, O. Vasiljeva, M. Renko, T. Sun, B. Turk, and D. Turk. 2012. Cysteine cathepsins: from structure, function and regulation to new frontiers. *Biochim. Biophys. Acta* 1824: 68–88.
8. Honey, K., and A. Y. Rudensky. 2003. Lysosomal cysteine proteases regulate antigen presentation. *Nat. Rev. Immunol.* 3: 472–482.
9. Müller, S., J. Dennemärker, and T. Reinheckel. 2012. Specific functions of lysosomal proteases in endocytic and autophagic pathways. *Biochim. Biophys. Acta* 1824: 34–43.
10. Delamarre, L., M. Pack, H. Chang, I. Mellman, and E. S. Trombetta. 2005. Differential lysosomal proteolysis in antigen-presenting cells determines antigen fate. *Science* 307: 1630–1634.
11. Delamarre, L., R. Couture, I. Mellman, and E. S. Trombetta. 2006. Enhancing immunogenicity by limiting susceptibility to lysosomal proteolysis. *J. Exp. Med.* 203: 2049–2055.
12. Moss, C. X., J. A. Villadangos, and C. Watts. 2005. Destructive potential of the aspartyl protease cathepsin D in MHC class II-restricted antigen processing. *Eur. J. Immunol.* 35: 3442–3451.
13. Bougnères, L., J. Helft, S. Tiwari, P. Vargas, B. H.-J. Chang, L. Chan, L. Campisi, G. Lauvau, S. Hugues, P. Kumar, et al. 2009. A role for lipid bodies in the cross-presentation of phagocytosed antigens by MHC class I in dendritic cells. *Immunity* 31: 232–244.
14. van Montfoort, N., M. G. Camps, S. Khan, D. V. Filippov, J. J. Weterings, J. M. Griffith, H. J. Geuze, T. van Hall, J. S. Verbeek, C. J. Melief, and F. Ossendorp. 2009. Antigen storage compartments in mature dendritic cells facilitate prolonged cytotoxic T lymphocyte cross-priming capacity. *Proc. Natl. Acad. Sci. USA* 106: 6730–6735.
15. Burgdorf, S., A. Kautz, V. Böhnert, P. A. Knolle, and C. Kurts. 2007. Distinct pathways of antigen uptake and intracellular routing in CD4 and CD8 T cell activation. *Science* 316: 612–616.
16. Lutz, M. B., N. Kukutsch, A. L. Ogilvie, S. Rössner, F. Koch, N. Romani, and G. Schuler. 1999. An advanced culture method for generating large quantities of highly pure dendritic cells from mouse bone marrow. *J. Immunol. Methods* 223: 77–92.
17. Joffre, O. P., E. Segura, A. Savina, and S. Amigorena. 2012. Cross-presentation by dendritic cells. *Nat. Rev. Immunol.* 12: 557–569.
18. Accapezzato, D., V. Visco, V. Francavilla, C. Molette, T. Donato, M. Paroli, M. U. Mondelli, M. Doria, M. R. Torrisi, and V. Barnaba. 2005. Chloroquine enhances human $CD8^+$ T cell responses against soluble antigens in vivo. *J. Exp. Med.* 202: 817–828.
19. Pasquevich, K. A., S. M. Estein, C. García Samartino, A. Zwerdling, L. M. Coria, P. Barrionuevo, C. A. Fossati, G. H. Giambartolomei, and J. Cassataro. 2009. Immunization with recombinant *Brucella* species outer membrane protein Omp16 or Omp19 in adjuvant induces specific $CD4^+$ and $CD8^+$ T cells as well as systemic and oral protection against *Brucella abortus* infection. *Infect. Immun.* 77: 436–445.
20. Pasquevich, K. A., A. E. Ibañez, L. M. Coria, C. García Samartino, S. M. Estein, A. Zwerdling, P. Barrionuevo, F. S. Oliveira, C. Seither, H. Warzecha, et al. 2011. An oral vaccine based on U-Omp19 induces protection against *B. abortus* mucosal challenge by inducing an adaptive IL-17 immune response in mice. *PLoS One* 6: e16203.
21. Coria, L. M., A. E. Ibañez, K. A. Pasquevich, P. L. Cobiello, F. M. Frank, G. H. Giambartolomei, and J. Cassataro. 2016. *Brucella abortus* Omp19 recombinant protein subcutaneously co-delivered with an antigen enhances antigen-specific T helper 1 memory responses and induces protection against parasite challenge. *Vaccine* 34: 430–437.
22. Létoffé, S., P. Delepelaire, and C. Wandersman. 1989. Characterization of a protein inhibitor of extracellular proteases produced by *Erwinia* chrysanthemi. *Mol. Microbiol.* 3: 79–86.
23. Wee, K. E., C. R. Yonan, and F. N. Chang. 2000. A new broad-spectrum protease inhibitor from the entomopathogenic bacterium Photorhabdus luminescens. *Microbiology* 146: 3141–3147.
24. Ibanez, A. E., L. M. Coria, M. V. Carabajal, M. V. Delpino, G. S. Risso, P. G. Cobiello, J. Rinaldi, P. Barrionuevo, L. Bruno, F. Frank, et al. 2015. A bacterial protease inhibitor protects antigens delivered in oral vaccines from digestion while triggering specific mucosal immune responses. *J. Control. Release* 220: 18–28.
25. Copeland, R. A. 2000. *Enzymes: A Practical Introduction to Structure, Mechanism, and Data Analysis.* Wiley, New York.
26. Copeland, R. A. 2005. *Evaluation of Enzyme Inhibitors in Drug Discovery: A Guide for Medicinal Chemists and Pharmacologists.* Wiley Interscience, Hoboken, NJ.
27. Toki, S., K. Goleniewska, M. M. Huckabee, W. Zhou, D. C. Newcomb, G. A. Fitzgerald, W. E. Lawson, and R. S. Peebles, Jr. 2013. PGI_2 signaling inhibits antigen uptake and increases migration of immature dendritic cells. *J. Leukoc. Biol.* 94: 77–88.
28. Drutman, S. B., and E. S. Trombetta. 2010. Dendritic cells continue to capture and present antigens after maturation in vivo. *J. Immunol.* 185: 2140–2146.
29. Tkach, M., L. Coria, C. Rosemblit, M. A. Rivas, C. J. Proietti, M. C. Díaz Flaqué, W. Beguelin, I. Frahm, E. H. Charreau, J. Cassataro, et al. 2012.

Targeting Stat3 induces senescence in tumor cells and elicits prophylactic and therapeutic immune responses against breast cancer growth mediated by NK cells and $CD4^+$ T cells. *J. Immunol.* 189: 1162–1172.
30. Lennon-Duménil, A. M., A. H. Bakker, R. Maehr, E. Fiebiger, H. S. Overkleeft, M. Rosemblatt, H. L. Ploegh, and C. Lagaudrière-Gesbert. 2002. Analysis of protease activity in live antigen-presenting cells shows regulation of the phagosomal proteolytic contents during dendritic cell activation. *J. Exp. Med.* 196: 529–540.
31. West, M. A., R. P. Wallin, S. P. Matthews, H. G. Svensson, R. Zaru, H. G. Ljunggren, A. R. Prescott, and C. Watts. 2004. Enhanced dendritic cell antigen capture via Toll-like receptor-induced actin remodeling. *Science* 305: 1153–1157.
32. Burgdorf, S., V. Lukacs-Kornek, and C. Kurts. 2006. The mannose receptor mediates uptake of soluble but not of cell-associated antigen for cross-presentation. *J. Immunol.* 176: 6770–6776.
33. Porgador, A., J. W. Yewdell, Y. Deng, J. R. Bennink, and R. N. Germain. 1997. Localization, quantitation, and in situ detection of specific peptide-MHC class I complexes using a monoclonal antibody. *Immunity* 6: 715–726.
34. Garulli, B., M. G. Stillitano, V. Barnaba, and M. R. Castrucci. 2008. Primary $CD8^+$ T-cell response to soluble ovalbumin is improved by chloroquine treatment in vivo. *Clin. Vaccine Immunol.* 15: 1497–1504.
35. Farady, C. J., and C. S. Craik. 2010. Mechanisms of macromolecular protease inhibitors. *ChemBioChem* 11: 2341–2346.
36. Savina, A., C. Jancic, S. Hugues, P. Guermonprez, P. Vargas, I. C. Moura, A. M. Lennon-Duménil, M. C. Seabra, G. Raposo, and S. Amigorena. 2006. NOX2 controls phagosomal pH to regulate antigen processing during cross-presentation by dendritic cells. *Cell* 126: 205–218.
37. Savina, A., A. Peres, I. Cebrian, N. Carmo, C. Moita, N. Hacohen, L. F. Moita, and S. Amigorena. 2009. The small GTPase Rac2 controls phagosomal alkalinization and antigen crosspresentation selectively in $CD8^+$ dendritic cells. *Immunity* 30: 544–555.
38. Rybicka, J. M., D. R. Balce, S. Chaudhuri, E. R. Allan, and R. M. Yates. 2012. Phagosomal proteolysis in dendritic cells is modulated by NADPH oxidase in a pH-independent manner. *EMBO J.* 31: 932–944.
39. Schnurr, M., M. Orban, N. C. Robson, A. Shin, H. Braley, D. Airey, J. Cebon, E. Maraskovsky, and S. Endres. 2009. ISCOMATRIX adjuvant induces efficient cross-presentation of tumor antigen by dendritic cells via rapid cytosolic antigen delivery and processing via tripeptidyl peptidase II. *J. Immunol.* 182: 1253–1259.
40. Cantisani, R., A. Pezzicoli, R. Cioncada, C. Malzone, E. De Gregorio, U. D'Oro, and D. Piccioli. 2015. Vaccine adjuvant MF59 promotes retention of unprocessed antigen in lymph node macrophage compartments and follicular dendritic cells. *J. Immunol.* 194: 1717–1725.
41. Segura, E., and J. A. Villadangos. 2009. Antigen presentation by dendritic cells in vivo. *Curr. Opin. Immunol.* 21: 105–110.
42. Dudziak, D., A. O. Kamphorst, G. F. Heidkamp, V. R. Buchholz, C. Trumpfheller, S. Yamazaki, C. Cheong, K. Liu, H. W. Lee, C. G. Park, et al. 2007. Differential antigen processing by dendritic cell subsets in vivo. *Science* 315: 107–111.
43. Hartmann, S., and R. Lucius. 2003. Modulation of host immune responses by nematode cystatins. *Int. J. Parasitol.* 33: 1291–1302.
44. Dainichi, T., Y. Maekawa, K. Ishii, T. Zhang, B. F. Nashed, T. Sakai, M. Takashima, and K. Himeno. 2001. Nippocystatin, a cysteine protease inhibitor from *Nippostrongylus brasiliensis*, inhibits antigen processing and modulates antigen-specific immune response. *Infect. Immun.* 69: 7380–7386.
45. Sun, Y., G. Liu, Z. Li, Y. Chen, Y. Liu, B. Liu, and Z. Su. 2013. Modulation of dendritic cell function and immune response by cysteine protease inhibitor from murine nematode parasite Heligmosomoides polygyrus. *Immunology* 138: 370–381.
46. De Gregorio, E., E. Caproni, and J. B. Ulmer. 2013. Vaccine adjuvants: mode of action. *Front. Immunol.* 4: 214.
47. Henrickson, S. E., T. R. Mempel, I. B. Mazo, B. Liu, M. N. Artyomov, H. Zheng, A. Peixoto, M. P. Flynn, B. Senman, T. Junt, et al. 2008. T cell sensing of antigen dose governs interactive behavior with dendritic cells and sets a threshold for T cell activation. *Nat. Immunol.* 9: 282–291.
48. Léonard, P., D. Nkoghe, M. Moutschen, and J. Demonty. 2001. [Pharma-clinics how I treat ... an HIV infection. IV. Protease inhibitors]. *Rev. Med. Liege* 56: 739–744.
49. Leung, D., G. Abbenante, and D. P. Fairlie. 2000. Protease inhibitors: current status and future prospects. *J. Med. Chem.* 43: 305–341.